THYROID
Volume 28, Number 6, 2018

DOI: 10.1089/thy.2018.0018

NFE2-Related Transcription Factor 2 Coordinates Antioxidant Defense with Thyroglobulin Production and Iodination in the Thyroid Gland

Panos G. Ziros,[1,2] Ioannis G. Habeos,[3] Dionysios V. Chartoumpekis,[4] Eleni Ntalampyra,[1,2] Emmanuel Somm,[1,2] Cédric O. Renaud,[1,2] Massimo Bongiovanni,[5] Ioannis P. Trougakos,[6] Masayuki Yamamoto,[7] Thomas W. Kensler,[4] Pilar Santisteban,[8] Nancy Carrasco,[9] Carrie Ris-Stalpers,[10] Elena Amendola,[11] Xiao-Hui Liao,[12] Luciano Rossich,[13,14] Lisa Thomasz,[13,14] Guillermo J. Juvenal,[13,14] Samuel Refetoff,[12,15,16] and Gerasimos P. Sykiotis[1,2]

Background: The thyroid gland has a special relationship with oxidative stress. While generation of oxidative substances is part of normal iodide metabolism during thyroid hormone synthesis, the gland must also defend itself against excessive oxidation in order to maintain normal function. Antioxidant and detoxification enzymes aid thyroid cells to maintain homeostasis by ameliorating oxidative insults, including during exposure to excess iodide, but the factors that coordinate their expression with the cellular redox status are not known. The antioxidant response system comprising the ubiquitously expressed NFE2-related transcription factor 2 (Nrf2) and its redox-sensitive cytoplasmic inhibitor Kelch-like ECH-associated protein 1 (Keap1) defends tissues against oxidative stress, thereby protecting against pathologies that relate to DNA, protein, and/or lipid oxidative damage. Thus, it was hypothesized that Nrf2 should also have important roles in maintaining thyroid homeostasis.

Methods: Ubiquitous and thyroid-specific male C57BL6J Nrf2 knockout (Nrf2-KO) mice were studied. Plasma and thyroids were harvested for evaluation of thyroid function tests by radioimmunoassays and of gene and protein expression by real-time polymerase chain reaction and immunoblotting, respectively. Nrf2-KO and Keap1-KO clones of the PCCL3 rat thyroid follicular cell line were generated using CRISPR/Cas9 technology and were used for gene and protein expression studies. Software-predicted Nrf2 binding sites on the thyroglobulin enhancer were validated by site-directed *in vitro* mutagenesis and chromatin immunoprecipitation.

Results: The study shows that Nrf2 mediates antioxidant transcriptional responses in thyroid cells and protects the thyroid from oxidation induced by iodide overload. Surprisingly, it was also found that Nrf2 has a dramatic impact on both the basal abundance and the thyrotropin-inducible intrathyroidal abundance of thyroglobulin (Tg), the precursor protein of thyroid hormones. This effect is mediated by cell-autonomous regulation of *Tg* gene expression by Nrf2 via its direct binding to two evolutionarily conserved antioxidant response elements in an upstream enhancer. Yet, despite upregulating Tg levels, Nrf2 limits Tg iodination both under basal conditions and in response to excess iodide.

[1]Service of Endocrinology, Diabetology and Metabolism; [5]Service of Clinical Pathology, Institute of Pathology; Lausanne University Hospital, Lausanne, Switzerland.
[2]Department of Physiology, Faculty of Biology and Medicine, University of Lausanne, Lausanne, Switzerland.
[3]Department of Internal Medicine, Division of Endocrinology, School of Medicine, University of Patras, Patras, Greece.
[4]Department of Pharmacology and Chemical Biology, University of Pittsburgh, Pittsburgh, Pennsylvania.
[6]Department of Cell Biology and Biophysics, Faculty of Biology, National and Kapodistrian University of Athens, Athens, Greece.
[7]Department of Medical Biochemistry, Tohoku University Graduate School of Medicine, Sendai, Japan.
[8]Instituto de Investigaciones Biomédicas Alberto Sols, Consejo Superior de Investigaciones Científicas y Universidad Autónoma de Madrid, CIBERONC (ISCIII), Madrid, Spain.
[9]Department of Cellular and Molecular Physiology, Yale School of Medicine, New Haven, Connecticut.
[10]Women's and Children's Clinic, Department of Obstetrics and Gynaecology, Academic Medical Center, University of Amsterdam, Amsterdam, The Netherlands.
[11]Dipartimento di Medicina Molecolare e Biotecnologie Mediche, Università degli Studi di Napoli, Federico II, Naples, Italy.
Departments of [12]Medicine and [15]Pediatrics and [16]Committee on Genetics, The University of Chicago, Chicago, Illinois.
[13]Nuclear Biochemistry Division, Argentine National Atomic Energy Commission, Buenos Aires, Argentina.
[14]CONICET, Buenos Aires, Argentina.

Conclusions: Nrf2 exerts pleiotropic roles in the thyroid gland to couple cell stress defense mechanisms to iodide metabolism and the thyroid hormone synthesis machinery, both under basal conditions and in response to excess iodide.

Keywords: Nrf2, thyroid, thyroglobulin, iodide, oxidative stress, animal testing alternatives

Introduction

OXIDATIVE STRESS (OS) ENSUES when reactive species overwhelm the cell's antioxidant and detoxification systems (1,2). In addition to protein and lipid damage, OS causes mutations and epigenetic perturbations, thereby leading to, or exacerbating, various diseases such as cancer, neurodegeneration, ischemia–reperfusion injury, chronic obstructive pulmonary disease, and many others. Disorders linked to oxidation affect tissues that are exposed to the environment (e.g., the skin, lung, and digestive tract), generate high amounts of free radicals (e.g., the muscle), function in detoxification (e.g., the liver, kidney, and placenta), or are particularly stress sensitive (e.g., neurons). In comparison, relatively little is known about the role of OS in the thyroid, an organ that generates high amounts of the oxidant hydrogen peroxide (H_2O_2) to oxidize iodide (I^-, the anion of iodine) and iodinate thyroglobulin (Tg) during the synthesis of thyroid hormones in the lumen of the spherical structures (follicles) formed by thyroid follicular cells. It has been shown that compared to other tissues, the thyroid has increased capacity to defend itself against OS (3). Specific antioxidant and detoxification enzymes have been identified that presumably help thyroid cells to maintain homeostasis by ameliorating oxidative insults, including glutathione peroxidase 2 (Gpx2) and thioredoxin reductase 1 (Txnrd1) (4,5). While a minimal oxidative load is necessary for normal thyroid cell function (6,7), the gland's antioxidant defense is activated by intrathyroidal OS occurring during iodide deficiency, goitrogenesis, or high iodide-induced involution of goiter (5,8,9). Yet, it is not well understood which systems allow thyrocytes to sense and respond to OS, and it is unknown whether the antioxidant defense mechanisms are coupled to the thyroid hormone synthesis process.

The ubiquitously expressed transcription factor NFE2-related transcription factor 2 (Nrf2) is a plausible candidate for mediating the thyroid's antioxidant response. In the absence of OS, Nrf2 binds to its cytoplasmic inhibitor Kelch-like ECH-associated protein 1 (Keap1) (10,11), which targets Nrf2 for poly-ubiquitination and subsequent proteasomal degradation. Keap1 also functions as a sensor of oxidants and electrophiles, which react with its redox-sensitive cysteines (12,13). Oxidative stressors abolish the inhibition of Nrf2 by Keap1; Nrf2 then accumulates in the nucleus where it transcriptionally activates protective genes through antioxidant response elements (AREs) in their regulatory sequences (14–16). Across the evolutionary spectrum, Nrf2 is required to defend organisms against OS and to protect against stress-related pathologies by preventing DNA, protein, and lipid oxidative damage (17), functioning as a multi-organ protector (18). In animal models of disease, pharmacological activation of Nrf2 by various synthetic and natural compounds can prevent cancer and other disorders linked to OS (19–21). Regarding the thyroid, a recent preliminary study suggested that Nrf2 is activated in the thyroid of rats in response to exposure to pharmacological doses of iodide, but the potential physiological relevance of this phenomenon was not addressed (22). Using ubiquitous and thyroid-specific Nrf2 knockout (Nrf2-KO) mice and Nrf2- or Keap1-KO thyroid follicular cell lines, this study shows that Nrf2 mediates antioxidant transcriptional responses in thyroid cells and protects the thyroid from oxidation induced by iodide overload. Surprisingly, the study also found that Nrf2 has a dramatic impact on both the basal abundance and the thyrotropin (TSH)-inducible abundance of Tg in the thyroid. This effect is mediated by direct, cell-autonomous regulation of *Tg* gene expression by Nrf2 via two evolutionarily conserved AREs. Thus, Nrf2 couples cell stress defense mechanisms to iodide metabolism and the thyroid hormone synthesis machinery.

Methods

Nrf2 knockout mice

C57BL/6J $Nrf2^{+/-}$ mice (15) were obtained from RIKEN BRC (Tsukuba, Japan). Nrf2 wild-type (WT) and knockout (Nrf2-KO) mice were generated by mating $Nrf2^{+/-}$ males and females. Offspring were genotyped, as previously described (15). For iodide challenge, male WT and Nrf2-KO mice (three to four months old) fed a standard diet were supplied with normal tap water with or without 0.05% sodium iodide (NaI) for seven days. Mice were housed in the animal facility of the University of Patras Medical School in temperature-, light-, and humidity-controlled rooms with a 12-hour light/dark cycle. All animal procedures were approved by the local Institutional Review Board and were in accordance with European Commission Directive 86/609/EEC.

Nrf2 thyroid-specific KO mice

Mice expressing Cre recombinase under control of the Pax8 locus (Pax8[Cre/+]) (23) were crossed with Nrf2 flox/flox mice that harbor flox sites flanking the DNA-binding domain (exon 5) of the *Nrf2* gene (24). The resulting Pax8(Cre/+)-Nrf2 flox/+ mice were backcrossed with Nrf2 flox/flox mice to obtain Pax8(Cre/+)-Nrf2 flox/flox mice, hereafter referred to as thyroid-specific Nrf2 KO (ts-KO). *Pax8* and *Nrf2* alleles were genotyped by polymerase chain reaction (PCR) using primers and conditions described in Supplementary Tables S1–S4 (Supplementary Data are available online at www.liebertpub.com/thy). Thyroid-specific *Nrf2* disruption as a result of recombination of the Nrf2 floxed allele was confirmed by genotyping thyroid DNA. Real-time reverse transcription (RT)-PCR was also used to confirm the thyroid-specific *Nrf2* deletion using primers targeting the exon 5 of *Nrf2* (Supplementary Table S5). Nrf2 flox/flox mice were used as a control group in experiments. Mice were housed in the animal facility of the Department of Physiology at the University of Lausanne

in temperature-, light-, and humidity-controlled rooms with a 12-hour light/dark cycle. All animal procedures were in accordance with Swiss legislature and approved by the Canton of Vaud SCAV.

Tissue collection

Mice were sacrificed by cervical dislocation immediately before removal of the thyroid gland. Thyroids were surgically dissected under a stereomicroscope and were immediately submerged in RNAlater solution for RNA and protein isolation or in 4% neutral-buffered formalin for tissue fixation and subsequent histology. Blood was collected with cardiac puncture.

Hormonal measurements

Plasma was collected using heparin- (Nrf2-KO mice and controls) or EDTA-coated tubes (ts-KO mice and controls) and was centrifuged at 2000 *g* for 20 min at 4°C. The difference in collection methods reflects the local practices in the respective laboratories (University of Patras and Lausanne University Hospital, respectively). Serum tests of thyroid function, including TSH, total thyroxine (T4) and total triiodothyronine (T3), were measured at the University of Chicago, as previously described in detail (25). Briefly, total T4 and T3 concentrations were measured in plasma with a coated tube radioimmunoassay (RIA) lit (Siemens Medical Solutions Diagnostics, Los Angeles, CA) adapted for mice using 25 and 50 μL of plasma, respectively. TSH was measured in 50 μL of plasma using a sensitive, heterologous, disequilibrium, double-antibody precipitation RIA. In one experiment (Nrf2-KO vs. WT, with or without NaI), total T4 was also measured at the University of Patras using an enzyme-linked immunosorbent assay kit (DET4105T100 Thyroxine (T4) Mouse/Rat; Demeditec Diagnostics, Kiel, Germany).

RNA isolation and real-time PCR

Total RNA from thyroid tissue and from cell lines was isolated using TRIzol (Invitrogen, Carlsbad, CA) and further purified using the RNeasy mini-kit with DNAse digestion (Qiagen, Valencia, CA). For thyroid tissue, cDNA was synthesized using 250 ng of RNA and the SuperScript VILO cDNA Synthesis Kit (Invitrogen). For cell lines, cDNA was synthesized using 500 ng of RNA and the PrimeScript cDNA Synthesis Kit (Takara Bio, Kusatsu, Japan). cDNA was diluted 20 times, and 5 μL was used for each reaction of 15 μL final volume. Real-time PCRs were performed on StepOnePlus or ViiA 7 Real-Time PCR System instruments (Applied Biosystems, Foster City, CA) using FAST SYBR green (Kapa Biosystems, Woburn, MA) under the following conditions: 3 min at 95°C, followed by 40 cycles of 10 s at 95°C and 25 s at 60°C. The primers used are shown in Supplementary Table S5. Melting curve analysis was used to confirm gene-specific amplification. Gene expression in thyroid tissues was quantified using relative standard curves derived from serial dilutions of pooled cDNAs with *Foxe1* as the reference gene. *Foxe1* was selected based on deep-sequencing data (not included in this study) showing no change in its expression levels between KO and WT mice with or without NaI treatment. Relative gene expression in cell lines was quantified by the comparative cycle threshold method using *Rpl19* as the reference gene.

Protein isolation, Western immunoblotting, immunohistochemistry, and analysis of protein oxidation

Total protein isolation from mouse thyroid tissues was performed with simple modifications of the TRIzol manufacturer's protocol published recently by the authors (26). Briefly, the manufacturer's protocol is followed until the precipitation of proteins from the phenol–ethanol supernatant, at which step the protein pellet is completely dissolved in 50–100 μL of 7 M GndCl solution, and then proteins are precipitated again by adding 1900 μL of 100% ethanol. This step is repeated, followed by a final wash of the protein pellet with 100% ethanol. After a 10 min air-drying period, the protein pellet is solubilized in 100–200 μL of buffer of 8 M urea, 40 mM of Tris, pH 8, 1% sodium dodecyl sulfate (SDS), and 1× Halt protease inhibitor cocktail (Thermo Fisher Scientific, Ecublens, Switzerland). Total protein extracts from PCCL3 cells were prepared using RIPA buffer (50 mM of Tris, pH 8, 150 mM of NaCl, 1% Nonidet P-40, 0.5% sodium deoxycholate, 0.1% SDS) supplemented with protease inhibitor cocktail and 5 μM of MG-132. Protein concentration in all samples was measured by the Pierce BCA protein assay kit (Thermo Fisher Scientific).

For Western blots, 20 μg (cell protein extracts) or 10 μg (thyroid protein extracts, 50 ng for the detection of Tg) was used, and they were performed as previously described (27) with minor modifications. Briefly, protein extracts were resolved on Bis-Tris-MOPS polyacrylamide gels or Tris-glycine sodium dodecyl sulfate polyacrylamide gel electrophoresis (SDS-PAGE), followed by electrotransfer onto polyvinylidene fluoride membranes (Amersham Biosciences, Little Chalfont, United Kingdom) with Tris-Bicine Transfer Buffer (25 mM of Bicine, 25 mM of Bis-Tris, 1 mM of EDTA, pH 7.2). Membranes were blocked at least 2 h with 5% nonfat dry milk in TBST (10 mM of Tris-HCl, pH 7.4, 150 mM of NaCl, 0.1% Tween 20), and incubated overnight with the indicated antibodies. After incubation with a horseradish peroxidase-conjugated secondary antibody, immunoreactive bands were visualized by WesternBright ECL (cell extracts) or WesternBright Sirius (tissue extracts) (Advansta, Menlo Park, CA), and recorded using a CCD image sensor (ChemiDoc XRS, Bio-Rad Laboratories, Cressier, Switzerland) or exposed to X-ray film (Fuji RX; Fujifim, Tokyo, Japan). The following primary antibodies were used: antithyroglobulin (A0251, 1:10,000; Dako, Glostrup, Denmark); anti-TG-I (28) (1:3000); anti-NIS (29) (1:5000); anti-Nrf2 (sc-13032, 1:1000; Santa Cruz Biotechnology, Dallas, TX); anti-BiP (3183, 1:1000; Cell Signaling Technology, Danvers, MA), anti-PERK (3192, 1:1000; Cell Signaling Technology); anti-Phospho-PERK (Thr980; 3179, 1:1000; Cell Signaling Technology); anti-SAPK/JNK (9252, 1:1000; Cell Signaling Technology); anti-Phospho-SAPK/JNK (Thr183/Tyr185; 9251, 1:1000; Cell Signaling Technology); anti-Atg12 (4180, 1:1000; Cell Signaling Technology); anti-Beclin-1 (3738, 1:1000; Cell Signaling Technology); anti-LC3B (2775, 1:1000; Cell Signaling Technology); anti-vinculin (SAB4200080, 1:5000; Sigma–Aldrich, St. Louis, MO), and anti-β-actin (4967, 1:5000; Cell Signaling Technology).

Secondary antibodies were anti-mouse HRP (#7076) and anti-rabbit HRP (#7074), both from Cell Signaling Technology (1:5000).

Immunohistochemistry was performed on slices from formalin-fixed paraffin-embedded thyroid tissues, as previously described (27), using primary antibodies against 4-hydroxynonenal (4-HNE; ab46545, 1:350; Abcam, Cambridge, United Kingdom) and cleaved caspase-3 (Asp175; 9661, 1:200; Cell Signaling Technology). Specific binding was detected with the Envision kit (Dako), and the color reaction was visualized with 3,3′-diaminobenzidine. For negative controls, blocking solution was added instead of primary antibody.

Protein oxidation in thyroid tissue extracts was evaluated by assaying the amount of carbonyl groups on proteins from pooled samples of each experimental group using the OxyBlot Protein Oxidation Detection kit (S7150; Merck Millipore, Billerica, MA) following the manufacturer's protocol. Briefly, 10 μg of protein samples were derivatized with 2,4-dinitrophenylhydrazine, and samples were loaded onto a 6% or 10% SDS-PAGE. Western immunoblotting was performed, as described above, using a specific antibody provided in the kit.

Cell culture

PCCL3 cells, a clonal rat thyroid cell line (30) were cultured in Coon's modified Ham's F-12 medium supplemented with 5% fetal bovine serum (FBS), 1% streptomycin/penicillin, and a six-hormone (6H) mixture comprising 0.5 mIU/mL of TSH, 10 μg/mL of insulin, 5 μg/mL of human Apo transferrin, 10 nM of hydrocortisone, 10 ng/mL of somatostatin, and 10 ng/mL of glycyl-L-histidyl-L-lysine acetate, hereafter referred to as 6H complete medium (30). Cells were cultured at 37°C, 5% CO_2, in a humidified incubator. Culture media and supplements were all from Sigma–Aldrich. The starvation medium, hereafter referred to as 4H medium, contained 0.2% FBS and four of the six hormones from the 6H medium (it lacked TSH and insulin). HeLa cells were cultured in Dulbecco's modified Eagle's medium supplemented with 10% (v/v) fetal calf serum.

Cell treatments

Unless otherwise stated, all chemicals were from Sigma–Aldrich. The following compounds were used for cell treatments: sulforaphane (SLF; R-1-isothiocyanato-4-methylsulfinylbutane) and CDDO-imidazole (CDDO-Im; 1-[2-cyano-3-,12-dioxooleana-1,9(11)-dien-28-oyl]imidazole) are Nrf2 activators; the latter was a gift from Prof. M. Sporn (Geisel School of Medicine, Dartmouth, NH) (31). Brusatol, an inhibitor of Nrf2 signaling, was a gift from Prof. D. Zhang (University of Arizona, Tucson, AZ) (32). OS conditions were induced using H_2O_2 or glucose oxidase (GOx); the latter generates H_2O_2 in the culture medium of the cells. NaI and the iodolipid 2-iodohexadecanal (2-IHDA) (33) were used to study the effects of iodide and its metabolites in cells.

Generation of stable ARE-Luc PCCL3 cell lines

A luciferase reporter plasmid (pNqo1-ARE-luc) bearing the ARE present in the 5′-flanking region of the rat *quinone reductase* gene (34,35) was used to create a stable PCCL3-ARE reporter cell line. PCCL3 cells plated into six-well plates 24 hours earlier were transfected with pNqo1-ARE-luc (500 ng), along with a pcDNA3.1 (50 ng) plasmid containing the neomycin selectable marker (Invitrogen) using a commercial transfection kit (jetPrime; Polyplus, Illkirch, France). Cells were split into 96-well plates 48 hours later and then selected using 500 μg/mL of G418 (Invitrogen) in the medium for three weeks. Resistant clones were isolated and screened by measuring their basal and inducible (obtained by treatment with 5 μM of sulforaphane; Enzo Life Sciences, Inc., Lausen, Switzerland) luciferase activities using the Luciferase Assay System (Promega, Madison, WI). A clone that displayed low background and high inducible luciferase activity was passaged and used in downstream experiments.

Promoter analysis and Tg promoter reporters

The promoter sequences for human and mouse Tg were downloaded from the EPDnew database (http://epd.vital-it.ch) (36) (Promoter ID: TG_1) and the rat promoter from NCBI GenBANK database (RefSeq: NC_005106.4). The JASPAR core database (http://jaspar.genereg.net) (37) was used to identify potential Nrf2 binding sites (ARE weight matrix, MA0150.2; relative score 0.80) in a 3.5 kb region upstream from the translation start site of the *Tg* gene. The previously described luciferase reporter vector hTGenh/prm-Luc (38) containing the human *Tg* upstream enhancer (39) and proximal basic *Tg* promoter (40) cloned upstream of the luciferase reporter gene of the PGL3 vector (hereafter, pTg) were used. The AREs were mutagenized, each one individually (pTg_mut_ARE1, pTg_mut_ARE2), as well as both together (pTg_mut_ARE1/2). The presence of ARE sequences in the enhancer region of the *Tg* promoter was confirmed by Sanger sequencing. The pTg vector was used as a template to create mutant versions of the core ARE sequences, named pTg_mut_ARE1 and pTg_mut_ARE2. Mutations were generated using the QuikChange II Site-Directed Mutagenesis Kit (Stratagene, San Diego, CA) following the manufacturer's protocol. After verification by Sanger sequencing, pTg_mut_ARE1 was used as a template to create the double mutant vector pTg_mut_ARE1/2. Primers used for mutagenesis and sequencing are listed in Supplementary Table S6.

RNA interference

Silencing of *Nrf2* and *Keap1* was performed using siRNAs from Santa Cruz Biotechnology (sc-156128 and sc-270459, respectively). The non-targeting negative control siRNA (sc-37007) was tested in parallel. PCCL3 cells were transfected either under starvation conditions (4H medium for 5 days) or under complete (6H) medium at a final siRNA concentration of 20 nM using Lipofectamine RNAiMax (Invitrogen). Compound treatments were performed 24 hours later, and cells were collected 48 hours after the siRNA transfections.

Chromatin immunoprecipitation

Cells grown in 15 cm dishes in complete 6H medium for 48 hours (after initial plating of four million cells) were treated with 5 μM of SLF or 0.1% dimethyl sulfoxide vehicle. Following 24 hours of treatment, cells were used for chromatin immunoprecipitation (ChIP) assays using the HighCell ChIP kit (Diagenode, Liege, Belgium) following the manufacturer's

instructions. A 1% portion of sheared cross-linked chromatin from each experimental condition was saved to serve as input DNA, and the rest was divided into equal parts and immunoprecipitated overnight at 4°C using 4 μg of rabbit-anti-Nrf2 polyclonal antibody (sc-13032 X; Santa Cruz Biotechnology) or 4 μg of rabbit IgG provided in the kit. Immunoprecipitated DNA were quantified by real-time RT-PCR using a standard curve from serial dilutions of input DNA and the primer pairs listed in Supplementary Table S7: (i) flanking the ARE1 sequence in the rat *Tg* promoter; (ii) flanking ARE2; (iii) flanking a validated ARE (positive control) in the rat *Nqo1* promoter (34); or (iv) targeting an unrelated sequence (negative control) about 350 bp downstream of the 5′ end of the *Actb* gene. Quantified DNA for each target was normalized to corresponding input DNA, and the results were plotted as fold enrichment of the target sequence versus the negative control.

Generation of PCCL3-ARE Nrf2 KO or Keap1 KO cells using CRISPR/Cas9

The PCCL3-ARE cells were used to inactivate the expression of *Nrf2* or *Keap1* using the CRISP/Cas9-mediated gene editing technology (41) and, specifically, the Edit-R gene editing system (Dharmacon, Inc., Lafayette, CO). Three different crRNAs (Supplementary Table S8) were tested for each target. Briefly, PCCL3-ARE cells grown in 12-well plates without antibiotics were transfected with 0.5 μg of Edit-R Cas9 expression plasmid (U-005100; Dharmacon, Inc.) using jetPrime transfection reagent. Twenty-four hours later, cells in each well were transfected again with a 10 pmol mixture of crRNA:tracrRNA complex (10 nM final concentration) and 1.7 μL of lipofectamine RNAiMAX in Optimem medium preincubated for 20 min at room temperature. Cells were trypsinized 48 h later and plated into six-well plates under puromycin selection for three more days. Surviving cells were split into 96-well plates (100 cells/plate) without puromycin, and single colonies were selected three weeks later. For *Nrf2* targeting, colonies were screened by measuring their basal and inducible (obtained by treatment with 5 μM of SLF) ARE-dependent luciferase activities. Colonies with very low background and with no response to SLF treatment were selected. For *Keap1* targeting, colonies were screened by measuring their basal luciferase activities. Colonies with at least threefold higher activity over the parental PCCL3-ARE cells were selected. Detection of frameshift mutations in the selected colonies was performed with Sanger sequencing on PCR-amplified DNA using primers flanking the target DNA sequence of each specific guide RNA (primers in Supplementary Table S9). Colonies with biallelic mutations (frameshift-causing single-base deletions of the target sequence) were selected. Homozygous *Nrf2* KO clones were named N2 and N3, and homozygous *Keap1* KO clones were named K1 and K3. A colony originating from an *Nrf2*-targeting crRNA that did not yield a mutation was used as a control in downstream experiments (originally N1, then relabeled WT).

Cell transfections and reporter assays

Transient transfections of cells with the different pTg reporters were performed in 96-well plates cultured in complete medium using a 1:2 ratio of DNA and jetPRIME transfection reagent, respectively. The pEGFP-N1 plasmid (Clontech, Mountain View, CA) was included for monitoring transfection efficiency, along with the Renilla pRLTK-ΔARE plasmid to normalize luciferase activities, as previously described (42).When the Nrf2-activating compounds SLF and CDDO-Im were used, they were applied 24 hours after transfection for the indicated times. In all transfections, the pEGFP-N1 plasmid (Clontech) was included for monitoring transfection efficiency 24 hours after transfection by examining cells under an Eclipse TS100 inverted fluorescence microscope (Nikon, Tokyo, Japan). Transfection efficiency was determined by the percentage of green fluorescent cells in the whole cell population. Experiments were performed only if transfection efficiency was the same between the different conditions. The Renilla pRLTK-ΔARE plasmid was used to normalize luciferase activities, as previously described (42). Cells were lysed 48 hours after transfection using Passive Lysis Buffer (Promega). The dual luciferase reporter assay (Promega) and a NOVOstar luminometer (BMG Labtech, Ortenberg, Germany) were used to measure luciferase activities according to the manufacturer's protocol. PCCL3 cells were transfected with 50 ng of total plasmid DNA per well as follows: 40 of WT pTg or the same quantity of indicated pTg_mut_ARE, 2 ng of pEGFP-N1, and 8 ng of pRLTK-ΔARE. HeLa cells were transfected with 35 ng of total plasmid DNA per well as follows: 12 of WT pTg or the same quantity of indicated pTg_mut_ARE, 0.5 ng of pEGFP-N1, 2.5 ng of pRLTK-ΔARE, 10 ng of pCDNA-Ttf1 (a gift from Prof. D. Mu (Eastern Virginia Medical School, Norfolk, VA), addgene plasmid #49989) (43), and 10 ng of pCDNA-Nrf2, pCDNA-Keap1, or pCDNA-mock (the latter three plasmids were kindly provided by Dr. N. Wakabayashi [University of Pittsburgh, Pittsburgh, PA]) (42).

General reactive oxygen species detection

The detection of endogenous reactive oxygen species (ROS) production was evaluated using the fluorescent probe CM-H_2DCFDA (Thermo Fisher Scientific). Briefly, cells were washed with Hank's balanced salt solution (HBSS) and incubated with 5 μM of CM-H_2DCFDA, along with 1 μM of Hoechst 33342 (Thermo Fisher Scientific) for 20 min at 37°C. Cell were then washed again with HBSS and allowed to recover for another 30 min at 37°C. Fluorescence was observed under an Eclipse TS100 microscope, and images were captured using a Digital Sight camera (Nikon).

Statistics

Results are presented in graphs as means ± standard deviation. Hormone levels were compared by two-way analysis of variance between WT and Nrf2 KO mice treated with NaI or not, testing for main effects (genotype, treatment), and interaction effects (genotype–treatment). Hormone levels were compared by unpaired *t*-test between WT and ts-KO mice. These statistical calculations were performed in GraphPad Prism v7 (GraphPad Software, Inc., La Jolla, CA), which was also used to prepare all graphs. For data calculated as normalized ratios (mRNA, protein, and luciferase quantifications), the BootstRatio application was used (http://rht.iconcologia.net/stats/br/index.html). This tool is based on bootstraping and resampling methods, without any assumption on the underlying probability distribution for the data analyzed (44). Whenever the same data were

used to test multiple hypotheses, a Bonferroni correction was applied as appropriate.

Results

Ubiquitous Nrf2 KO mice demonstrate that Nrf2 mediates protective antioxidant responses to iodide overload and impacts Tg expression and iodination levels

Under normal conditions, Nrf2 KO mice showed similar TSH levels as WT mice, indicating a euthyroid state (Fig. 1A). In both genotypes, TSH levels increased significantly and to a similar extent after iodide overload for one week (Fig. 1A). Genotype, treatment, and their interaction had no significant impact on total T3 levels (Fig. 1B). Total T4 levels, which decreased significantly in both genotypes in response to iodide, were slightly higher in the Nrf2 KO mice compared to WT mice both under basal conditions and after iodide overload (Fig. 1C). This was confirmed in an independent cohort of animals (Fig. 1D). The genotype–treatment interaction did not show a significant effect for any of the three hormones. Together, these data indicate that Nrf2 KO mice show, compared to WT mice, only minor differences in thyroid function tests under basal conditions, notably in total T4 levels. The absolute magnitude of these differences is small, and they are not accompanied by a significant difference in TSH levels, indicating normal overall thyroid function. Moreover, the physiological hormonal response to excess iodide is largely preserved in Nrf2 KO mice under the conditions employed.

The study validated that Nrf2 KO mice show no expression of Nrf2 in their thyroid glands, and found that iodide overload had no effect on *Nrf2* mRNA levels in WT mice (Fig. 1E). Expression levels of the prototypical Nrf2 target gene, *Nqo1*, were significantly lower in Nrf2 KO mice compared to WT mice both under basal conditions and after iodide challenge (Fig. 1F). Moreover, *Nqo1* mRNA levels were significantly upregulated by iodide treatment in WT mice, while no induction was observed in KO mice (Fig. 1F), indicating that iodide activates the Nrf2 antioxidant response in the thyroid gland. The mRNA levels of *Gpx2* (Fig. 1G) showed the same statistically significant patterns as *Nqo1*, indicating that this gene is also upregulated by iodide in a Nrf2-dependent manner. A similar but not statistically significant pattern was observed for *Txnrd1* mRNA levels (Fig. 1H). Under both basal and iodide overload conditions, *Tg* mRNA levels were markedly lower in Nrf2 KO mice compared to WT (Fig. 1I). As expected (45), *Nis* mRNA levels were significantly reduced in response to iodide in WT mice. This response was preserved in Nrf2 KO mice (Fig. 1J). A trend toward lower *Nis* mRNA levels was observed in Nrf2 KO mice compared to WT, which was statistically significant under iodide overload conditions (Fig. 1J). The expression levels of other thyroid-specific genes are shown in Supplementary Figure S1A–J. Overall, these data demonstrate that Nrf2 mediates thyroidal antioxidant responses to iodide and that it has a major impact on *Tg* mRNA levels independently of iodide. Thus, subsequent investigations were focused on elucidating the mechanisms involved.

At the protein level, *Nqo1* was detectable only in WT mice exposed to iodide, while it was undetectable under basal conditions in WT mice, as well as in Nrf2 KO mice in either condition (Fig. 1K and Supplementary Fig. S2). This pattern is consistent with the respective mRNA expression levels (Fig. 1F). When the total oxidized protein content was assayed, WT mice showed a mild decrease in response to iodide overload (Fig. 1L). This is compatible with a known autoregulatory response whereby H_2O_2 levels decrease in response to high iodide (46). On the other hand, Nrf2 KO mice showed a mild increase in total protein oxidation under basal conditions, as well as a clear increase after iodide challenge (Fig. 1L), suggesting a dysfunction in this autoregulatory mechanism. Challenging Nrf2 KO mice with iodide also caused a clear increase in immunostaining for the oxidized lipid product 4-HNE in thyroid follicular cells (Fig. 1M). Together, these data indicate that the Nrf2-mediated antioxidant response protects the thyroid gland from iodide overload-induced oxidative damage. Overall, no major gross morphological abnormalities were observed among the groups, but a detailed histomorphological characterization of the thyroids of Nrf2-KO mice (and other Nrf2-KO vertebrate models) is in progress. Immunohistochemistry for cleaved caspase 3 showed very low levels of apoptosis in WT mice under normal conditions, as well as in the various experimental groups (Supplementary Fig. S3). The number of follicles that harbored at least one cleaved caspase 3-positive cell ranged from 0% to 1% in all groups.

Consistent with the pattern of *Tg* mRNA levels (Fig. 1I), Tg protein levels were significantly lower in Nrf2 KO mice compared to WT mice, both under basal conditions (Fig. 2A, C, D, F, and P) and in response to iodide challenge (Fig. 2B, C, E, F, and T). On the contrary, iodinated Tg (I-Tg) levels were significantly higher in Nrf2 KO mice compared to WT mice under basal conditions (Fig. 2G, I, Q, and R). Moreover, whereas I-Tg levels decreased in WT mice in response to iodide overload, they increased significantly in Nrf2 KO mice (Fig. 2G–I, U, and V). These data suggest that the iodide overload-induced inhibition of Tg iodination (the Wolff–Chaikoff phenomenon) (47) is dysfunctional in Nrf2 KO mice. On the other hand, NIS protein levels appropriately decreased in both WT and Nrf2 KO mice (Fig. 2J–L, S, and W), indicating that the escape mechanism from the Wolff–Chaikoff phenomenon (45) is not dependent on Nrf2. Taken together, these data show clear effects of Nrf2 on the protein levels of Tg and its iodinated form, indicating partial dysfunction of the iodide-handling mechanisms in thyrocytes. The main results of the above-described mouse experiments among the different genotypes and conditions are summarized in Table 1.

Thyroid-specific Nrf2 KO mice show that the effects of Nrf2 on antioxidant genes and Tg are thyroid autonomous

To distinguish which of the aforementioned effects of Nrf2 are thyroid autonomous and which are mediated by actions of Nrf2 in peripheral tissues, thyroid-specific (ts-)Nrf2 KO mice (Pax8-Cre/+, Nrf2 flox/flox) were generated, and they were compared to littermate control Nrf2 flox/flox mice under basal conditions. The levels of plasma TSH, total T4, and total T3 were similar between the two genotypes (Fig. 3A–C), indicating that the observed difference in total T4 levels between ubiquitous Nrf2 KO and WT mice (Fig. 1C and D) is likely due to extrathyroidal effects of Nrf2 on the transport or

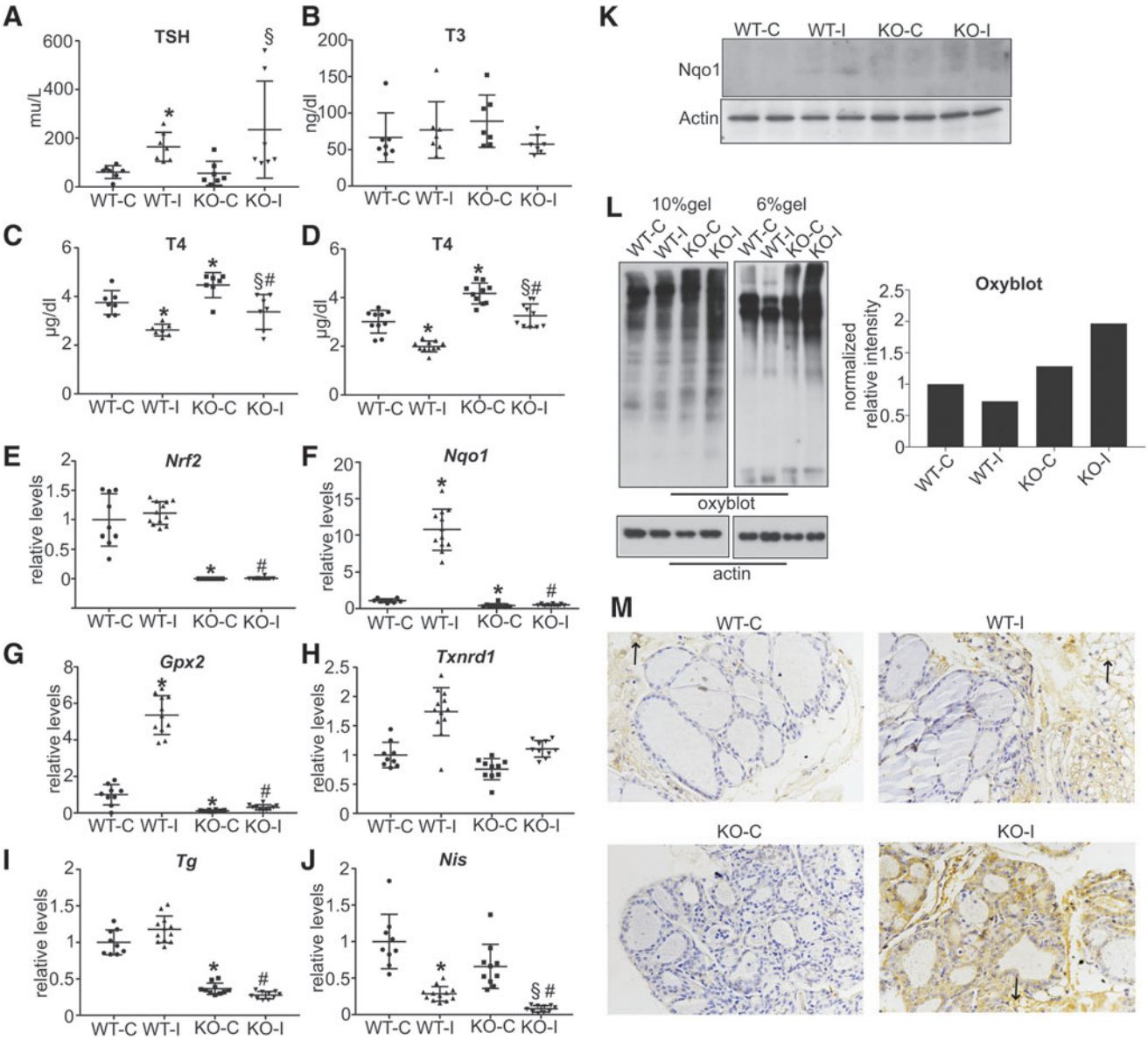

FIG. 1. Thyroid function tests, relative thyroidal gene expression levels, thyroidal Nqo1 protein levels, and thyroidal oxidized protein levels of wild-type (WT) and NFE2-related transcription factor 2 (Nrf2) knockout (KO) male mice under basal conditions and after iodide overload. Three- to four-month-old male mice were supplied for seven days with normal water (-C) or with 0.05% sodium iodide (NaI) in their drinking water (-I). (**A**) Plasma thyrotropin (TSH), (**B**) total triiodothyronine (T3), and (**C**) total thyroxine (T4) were measured by radioimmunoassay (RIA) in WT-C, WT-I, KO-C, and KO-I mice (seven mice per group). (**D**) Plasma total T4 was measured by enzyme-linked immunosorbent assay in an independent cohort of animals (10 mice per group). (**E**) *Nrf2* (**F**) *Nqo1* (**G**) *Gpx2* (**H**) *Txnrd1* (**I**) *Tg*, and (**J**) *Nis* mRNA levels were quantified by real-time reverse transcription polymerase chain reaction (RT-PCR) in WT-C ($n=9$), WT-I ($n=12$), KO-C ($n=10$), and KO-I ($n=10$) mice. Results for each mouse are presented as relative quantity over the mean of the WT-C group. Error bars indicate means ± standard deviation. $^{*}p<0.05$ vs. WT-C; $^{\S}p<0.05$ vs. KO-C; $^{\#}p<0.05$ vs. WT-I. (**K**) Nqo1 protein levels were assayed by Western immunoblotting in thyroid protein extracts from WT-C, WT-I, KO-C, and KO-I mice (seven mice per group). A pooled sample from each group was run in duplicate (two lanes per group). As controls for protein loading, the membranes were stripped and re-probed with an anti-actin antibody and then also stained with Coomassie blue. (**L**) As an index of oxidative stress, protein carbonyl content was assayed using the OxyBlot Protein Oxidation Detection kit. Pooled protein thyroid extracts from the same animals were treated accordingly then separated on a 6% or a 10% gel, and detection of carbonyl protein modifications was performed by Western immunoblotting. The membranes were stripped and re-probed with an anti-actin antibody and then also stained with Coomassie blue. Densitometric quantification of relative protein carbonyls in the different groups was performed using Image-J software. The graph shows relative band intensity normalized to the corresponding actin band and to the WT-C group. (**M**) Immunohistochemical staining for 4-HNE in representative thyroid slices each group. Arrows indicate positive control staining in fat tissue.

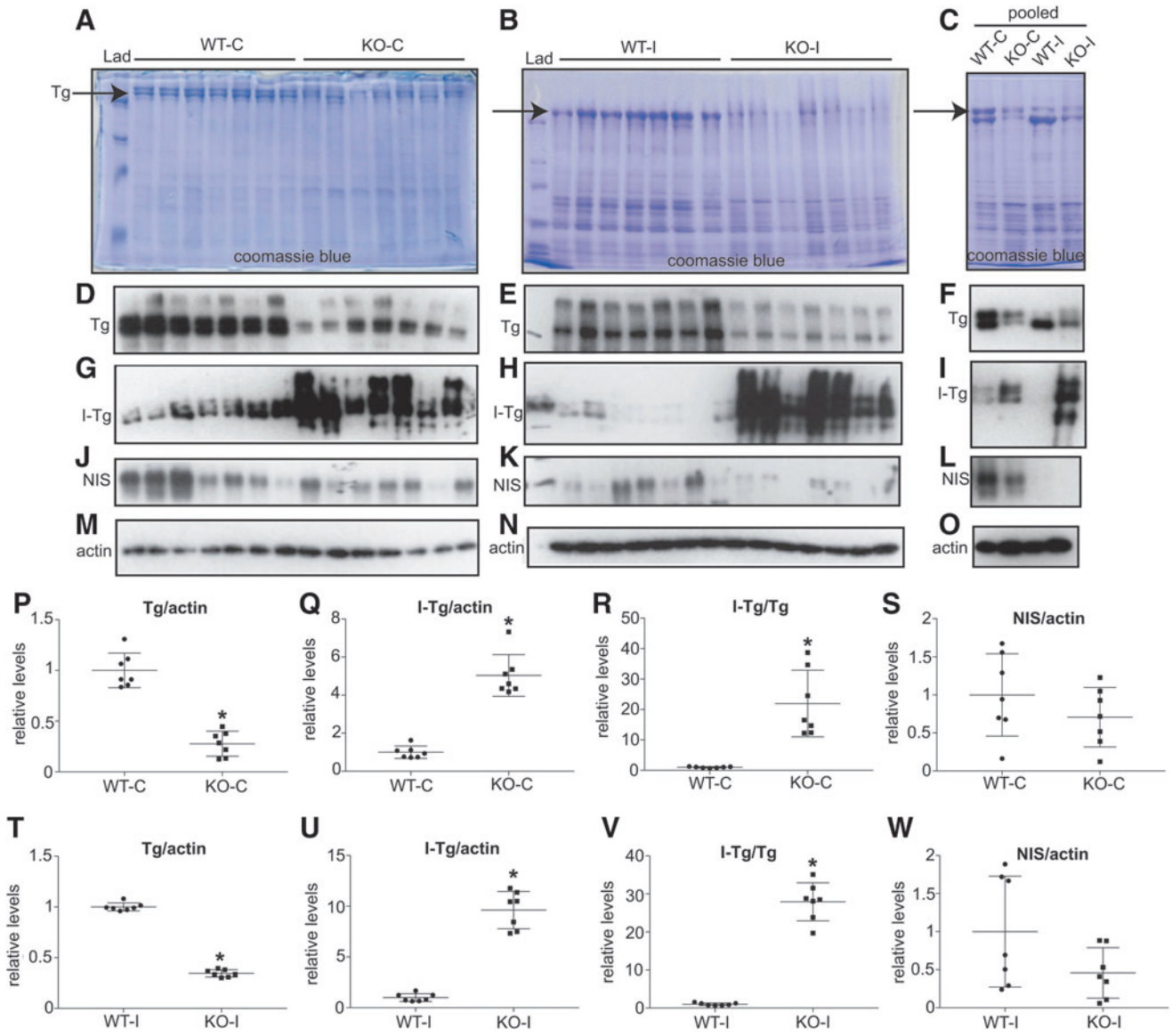

FIG. 2. Thyroglobulin (Tg), iodinated Tg (I-Tg), and NIS protein levels in thyroids of WT and Nrf2 KO male mice under basal conditions and after iodide overload. Sodium dodecyl sulfate polyacrylamide gel electrophoresis (SDS-PAGE) and Coomassie blue staining of thyroid protein extracts from individual animals (WT-C, KO-C, WT-I, and KO-I; seven mice per group) under basal conditions (**A**) or after iodide treatment (**B**) and in respective pooled extracts (**C**). Western immunoblotting for Tg (**D**, **E**, and **F**), I-Tg (**G**, **H**, and **I**), NIS (**J**, **K**, and **L**), and actin (**M**, **N**, and **O**). Lad indicates protein ladder size marker. (**P**–**W**) Densitometric quantification of relative protein levels in the different mice was performed using ImageJ, with normalization to the respective actin levels and to the appropriate control group (WT-C or WT-I). Error bars indicate means ± standard deviation. $*p < 0.05$.

TABLE 1. SUMMARY OF THE MAIN FINDINGS IN MICE

	WT-I	*Nrf2 KO-C*	*Nrf2 KO-I*
Tg mRNA	–	↓	↓
Tg protein	↓	↓	↓
Iodinated Tg	↓	↑	↑↑
Nqo1 (*Gpx2*, *Txrnd1*) mRNA	↑	↓	↓
Oxidized proteins	–	–	↑
Oxidized lipids	–	–	↑

Arrows indicate changes compared to WT-C mice; –, unchanged. WT, wild type; KO, knockout; Tg, thyroglobulin.

peripheral metabolism of T4. The mean *Nrf2* mRNA levels in the ts-Nrf2 KO mice were 7.5% of WT levels (range 4.9–10%; Fig. 3D). Given that the thyroids of these animals also contain cells that are WT for Nrf2 (e.g., endothelial cells, blood cells, fibroblasts, adipocytes, etc.), it was concluded that the efficiency of the knockout is >90%. Importantly, these mice recapitulated the differences observed in ubiquitous Nrf2 KO mice in the basal expression levels of antioxidant genes (Fig. 1F–H), showing significantly lower mRNA levels of *Nqo1* (Fig. 3E) and *Gpx2* (Fig. 3F) as well as of *Txnrd1* (Fig. 3G). Similarly to ubiquitous Nrf2 KO mice (Fig. 1I), they also showed markedly lower mRNA

levels of *Tg* compared to controls (Fig. 3H). *Nis* mRNA levels were also significantly lower (Fig. 3I), consistent with the nonsignificant trend observed in ubiquitous Nrf2 KO mice (Fig. 1J). Gene expression levels of other thyroid-specific genes are shown in Supplementary Figure S1K–T.

At the protein level, Tg was significantly less abundant in the thyroids of ts-Nrf2 KO mice in basal conditions compared to controls (Fig. 3J, K, and O). Conversely, the levels of iodinated Tg were higher in ts-Nrf2 KO mice (Fig. 3L and P), and the ratio of iodinated to total Tg was markedly higher in ts-Nrf2 KO mice compared to controls (Fig. 3Q). Thus, ts-Nrf2 KO mice under basal conditions recapitulate the phenotype of ubiquitous Nrf2 KO mice regarding lower mRNA expression of antioxidant genes, lower mRNA expression, and protein abundance of Tg, as well as higher levels of Tg iodination, which indicates that these effects are mediated via actions of Nrf2 in the thyroid gland.

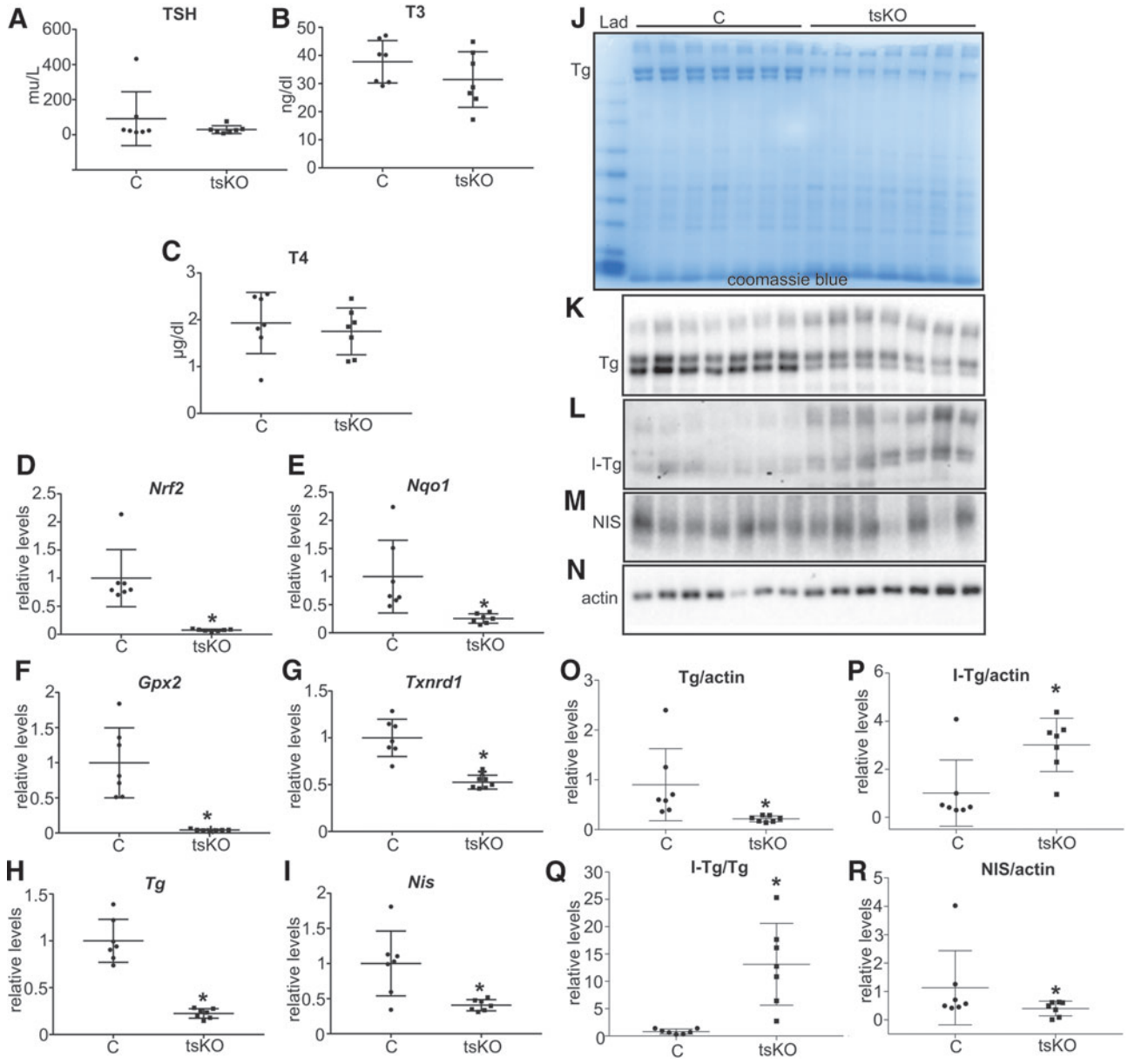

FIG. 3. Thyroid function tests, relative thyroidal gene expression levels, and Tg, I-Tg, and NIS protein levels in control (C, Nrf2 flox/flox) and thyroid-specific (ts-) Nrf2 KO male mice under basal conditions. Plasma TSH (**A**), total T3 (**B**), and total T4 (**C**) were measured by RIA in three- to four-month-old C and ts-Nrf2 KO mice (seven mice per group). *Nrf2* (**D**), *Nqo1* (**E**), *Gpx2* (**F**), *Txnrd1* (**G**), *Tg* (**H**), and *Nis* (**I**) mRNA levels were quantified by real-time RT-PCR. Results for each mouse are presented as relative quantity over the mean of the C group. (**J**) SDS-PAGE and Coomassie blue staining of thyroid protein extracts from individual animals. Western immunoblotting for Tg (**K**), I-Tg (**L**), NIS (**M**), and actin (**N**). Lad indicates protein ladder size marker. (**O**–**R**) Densitometric quantification of relative protein levels in the different mice was performed using Image-J, with normalization to the respective actin levels and to the C group. Error bars indicate means ± standard deviation. $*p < 0.05$.

Nrf2 regulates antioxidant responses, as well as the basal and TSH-inducible Tg levels, in a cell-autonomous manner

To characterize further the thyroidal effects of Nrf2 on antioxidant responses and Tg levels and to associate them definitively with the thyroid follicular cells, first *Nrf2* was knocked down in the PCCL3 rat thyroid follicular cell line using RNA interference. The efficiency of the knockdown under the various conditions employed is shown in Supplementary Figure S4A, B, G, and H. Knockdown of *Nrf2* significantly decreased the mRNA levels of *Nqo1* under basal conditions (Supplementary Fig. S4C), under starvation conditions (Fig. 4A), and in response to TSH re-treatment (Fig. 4A). Conversely, knockdown of *Keap1* significantly increased the mRNA levels of *Nqo1* under basal conditions (Supplementary Fig. S4C) and under starvation conditions (Fig. 4A). Regarding Tg, knockdown of *Keap1* clearly increased its mRNA levels under basal conditions (Supplementary Fig. S4D) and under starvation conditions (Fig. 4B), while knockdown of *Nrf2* significantly decreased *Tg* mRNA levels in response to TSH stimulation (Fig. 4B) but not its basal expression levels (Supplementary Fig. S4D), indicating that even low Nrf2 expression levels (Supplementary Fig. S4A) can maintain physiological Tg expression. Having verified that treatment of PCCL3 cells with pharmacological activators of Nrf2 (CDDO-Im [CD for short] and SLF) stabilizes Nrf2 and increases Tg protein levels in cells starved in the presence of TSH or TSH plus insulin (Supplementary Fig. S4K), it was found that the knockdown of *Nrf2* clearly decreased the inducible protein levels of Tg (Fig. 4C). Conversely, the knockdown of *Keap1* tended to increase the inducible protein levels of Tg under the same conditions (Fig. 4C).

Based on these findings under partial genetic loss- or gain-of-function conditions, CRISPR/Cas9 gene editing was then employed to generate PCCL3 rat cell lines KO for *Nrf2* (named N2 and N3) or for *Keap1* (named K1 and K3). Clones were validated by Sanger sequencing genetically and also functionally after pharmacological stimulation with SLF, as it was found that SLF stabilized Nrf2 in WT cells but not in Nrf2 KO cells. Conversely, Nrf2 was constitutively activated

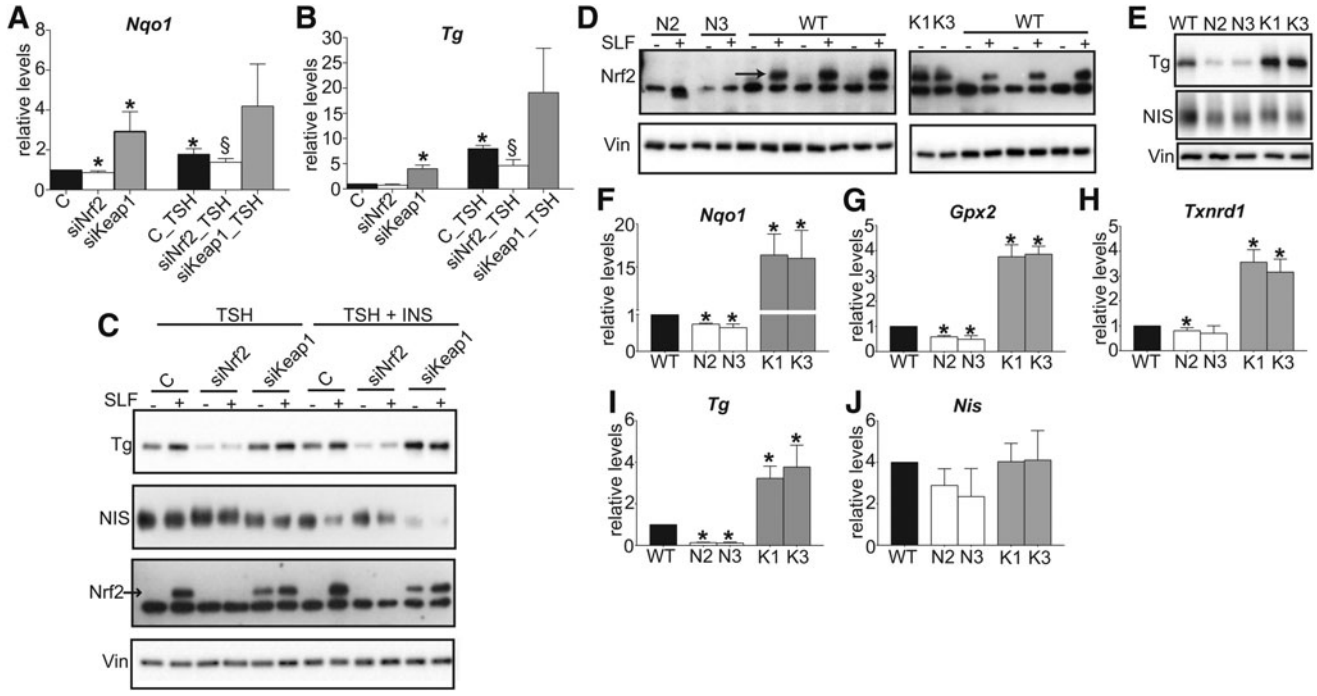

FIG. 4. Small interfering RNA (siRNA)-mediated silencing or CRISPR/Cas9-mediated knockout of Nrf2 and Keap1 in PCCL3 cells. (**A**–**C**) PCCL3 rat thyroid cells maintained for five days under starvation conditions (4H medium without TSH and insulin) were transfected as indicated with siRNAs targeting Nrf2 or Keap1 or a non-targeting control oligonucleotide (''C''). Cells were treated 24 hours later as indicated with 0.5 mIU/mL of TSH or with TSH and 10 μg/mL of insulin (INS) with or without sulforaphane (SLF) for another 24 hours. Relative mRNA levels of *Nqo1* (**A**) and *Tg* (**B**) normalized to *Rpl19* as the reference gene were quantified by real-time RT-PCR. Error bars indicate means ± standard deviation of at least three independent experiments. $^{*}p < 0.05$ vs. C; $^{\S}p < 0.05$ vs. C_TSH. (**C**) Western blot analysis of Tg, NIS, Nrf2, and vinculin (Vin) as a loading control. (**D**–**J**) CRISP/Cas9-mediated gene editing was used to create stable PCCL3 cell clones with targeted homozygous inactivation of Nrf2 (clones N2 and N3) or Keap1 (clones K1 and K3). (**D**) Western immunoblotting analysis of Nrf2 expression under basal conditions (complete culture medium) or after pharmacological Nrf2 activation with SLF (5 μM) for 24 hours. The arrow indicates the specific Nrf2 protein band. WT denotes different cell clones with no disruption of Nrf2 or Keap1, selected under the same conditions as the KO clones. Vin served as loading control. (**E**) Western immunoblotting analysis of Tg and NIS abundance in WT and KO cell lines under basal conditions (complete culture medium). Relative mRNA expression levels of *Nqo1* (**F**), *Gpx2* (**G**), *Txnrd1* (**H**), *Tg* (**I**), and *Nis* (**J**) normalized to *Rpl19* as the reference gene were quantified by real-time RT-PCR in cells cultured as above. Error bars indicate means ± standard deviation of at least three independent experiments. $^{*}p < 0.05$ vs. WT.

in Keap1 KO cells (Fig. 4D). Under basal conditions, *Tg* mRNA and protein levels were markedly lower in Nrf2 KO cells and higher in Keap1 KO cells (Fig. 4E and I). The same pattern was observed in the mRNA expression levels of antioxidant genes (Fig. 4F–H), with lower basal levels of *Nqo1*, *Gpx2*, and *Txnrd1* mRNA in Nrf2 KO cells and higher levels in Keap1 KO cells. *Nis* showed a non-significant tendency for lower mRNA levels in Nrf2 KO cells (Fig. 4J). Expression levels of other thyroidal genes are shown in Supplementary Fig. S4L–Q. Compared to the differences in Tg levels, in those cases when differences in other thyroidal genes were observed, they were of small magnitude, inconsistent between the two lines of the same genotype, and/or similar between Nrf2 KO cells and Keap1 KO cells, suggesting that among thyroid-specific genes, only *Tg* was likely to be under direct regulation by Keap1/Nrf2 signaling.

Then, the same parameters were assayed in response to starvation followed by stimulation by either TSH or TSH plus insulin. Tg protein levels were undetectable after starvation in WT cells (Fig. 5A). This has been previously described and is considered a result of a general quiescence of the cells in the absence of TSH and insulin/IGF-1 signaling (48,49). In WT cells, TSH re-treatment induced detectable levels of Tg. In contrast, stimulated Tg was hardly detectable in TSH-re-treated Nrf2 KO cells (Fig. 5A). Conversely, high levels of Tg were detectable in Keap1 KO cells under starvation conditions, with further induction upon TSH re-treatment (Fig. 5A). Similar differences were observed when starved cells were treated with both TSH and insulin (Fig. 5B), the latter being known to yield a more potent induction of Tg compared to TSH treatment alone (48). The differences in inducible Tg levels observed after 24 hours of treatment also persisted after a more prolonged stimulation of the cells for 48 hours (Supplementary Fig. S5A). Of note, the patterns of Tg expression in the cell culture media matched very well the patterns of the respective cellular extracts, suggesting that the differences observed between genotypes were not due to altered export of Tg (Supplementary Fig. S6). Moreover, overexposure of the blots from cell extracts did not reveal more Tg bands of lower molecular weight in the Nrf2 KO cells. This would argue against excessive Tg degradation in these cells (Supplementary Fig. S6). Similarly, overexposure of the blots from mouse thyroid extracts did not reveal more Tg bands of lower molecular weight in the ts-Nrf2 KO mice compared to control mice (Supplementary Fig. S7), arguing against increased Tg degradation *in vivo* as well. Finally, Western immunoblotting for various markers of endothelial reticulum stress (BIP, pERK, and pJNK) or autophagy (Beclin, ATG12-ATG5, and Lc3b) did not suggest differences in the activation status of these stress pathways between WT cells, Nrf2 KO cells and Keap1 KO cells (Supplementary Fig. S8).

Consistent with the Tg protein expression patterns, both the basal and the inducible *Tg* mRNA levels were also markedly lower in Nrf2 KO cells and higher in Keap1 KO cells (Fig. 5C). Interestingly, TSH- or TSH and insulin-inducible *Nis* mRNA and protein levels were lower in Keap1 KO cells (Fig. 5A and D) compared to WT cells. The expression patterns of other thyroidal genes are shown in Supplementary Figure S5B–N. The mRNA expression patterns of antioxidant genes (*Nqo1*, *Gpx2*, and *Txnrd1*) are consistent with regulation by the Keap1/Nrf2 pathway

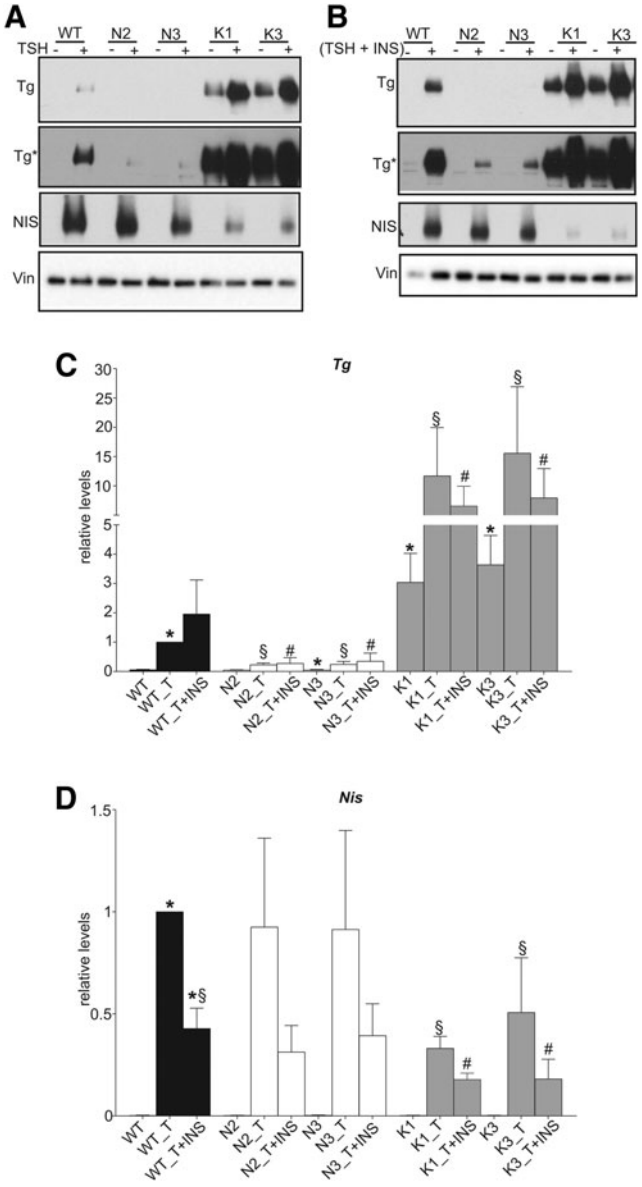

FIG. 5. Impact of Nrf2 or Keap1 knockout on TSH-inducible thyroid-specific protein and gene expression in PCCL3 cells. PCCL3 WT or KO cells maintained for five days under starvation conditions (4H medium without TSH and insulin) were stimulated with 0.5 mIU/mL of TSH (**A**) or 0.5 mIU/mL of TSH and 10 μg/mL of insulin (**B**) for 24 hours. (**A** and **B**) Western immunoblotting for Tg, NIS, and Vin as a loading control was performed using total protein extracts from the above conditions. The asterisk (*) indicates intentional overexposure of the Tg immunoblot to visualize the faint bands in the Nrf2 KO clones. Relative mRNA levels of *Tg* (**C**) and *Nis* (**D**) normalized to the *Rpl19* reference gene were quantified by real-time RT-PCR. T, TSH; INS, insulin. Error bars indicate means ± standard deviation of at least three independent experiments. $^{*}p < 0.05$ vs. WT; $^{\S}p < 0.05$ vs. WT_T; $^{\#}p < 0.05$ vs. WT_T + INS.

under TSH and/or TSH and insulin stimulation conditions (Supplementary Fig. S5B–D). In conclusion, these data demonstrate that the Keap1/Nrf2 pathway has an impact on the expression levels of antioxidant genes, as well as on the basal and inducible levels of Tg in thyroid follicular cells. Given the known functions of Nrf2 in other tissues, regulation of antioxidant genes in the thyroid was highly plausible. Yet, the relationship with iodide warranted further investigation. Moreover, regulation of Tg, a tissue-specific protein, by a ubiquitous transcription factor like Nrf2 was a highly intriguing finding, prompting the underlying mechanisms to be elucidated.

Iodide and its active metabolite 2-IHDA regulate ARE-mediated transcription in thyroid follicular cells

To investigate mechanisms of transcriptional regulation by Nrf2, PCCL3 cells stably transfected with an ARE-luciferase reporter construct (PCCL3-ARE cells) were employed. Preliminary experiments verified that this reporter responded in a dose-dependent manner to treatment with pro-oxidant substances such as glucose oxidase (GOx) and H_2O_2 (Supplementary Fig. S9A) or with the Nrf2 activator CDDO-Im (Supplementary Fig. S9C). Moreover, the Nrf2 inhibitor brusatol decreased the basal, H_2O_2-inducible, and CDDO-Im-inducible reporter activity in a dose-dependent manner (Supplementary Fig. S9B and D). Reporter activity was also significantly induced by treatment with TSH and insulin, whereas it was slightly suppressed by TSH alone (Supplementary Fig. S9E).

When WT PCCL3-ARE cells were treated with iodide, reporter activity increased significantly. This induction was completely blocked by concurrent treatment with the free radical scavenger NAC, which also reduced significantly the basal reporter activity (Fig. 6A). In contrast, neither iodide nor NAC had any effect on reporter activity in Nrf2 KO PCCL3-ARE cells. Also, in these cells, the basal ARE activity was significantly reduced compared to WT PCCL3-

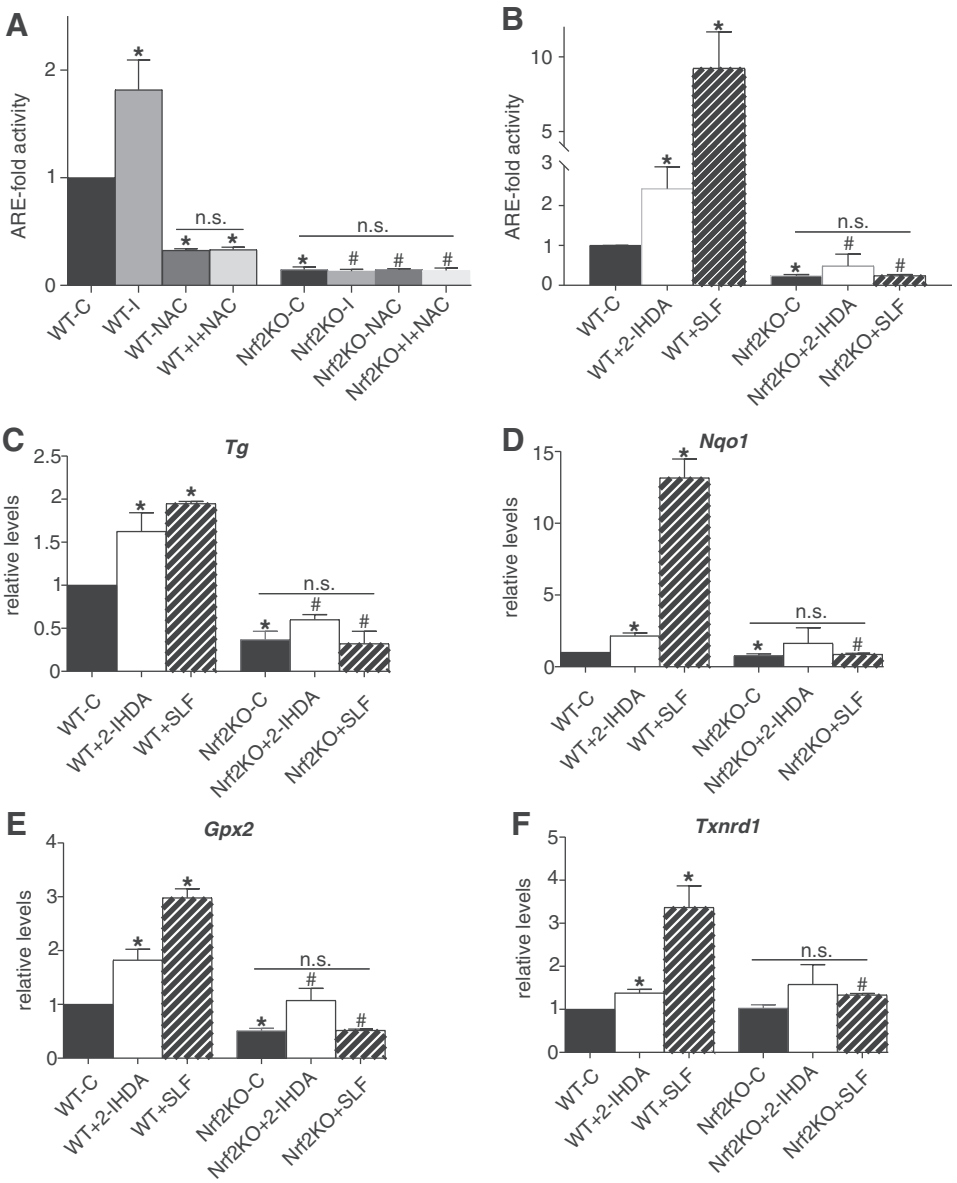

FIG. 6. Effects of iodide and 2-iodohexadecanal (2-IHDA) on Nrf2-mediated ARE activity and target gene transcription. Equal numbers of PCCL3 ARE-WT or ARE-Nrf2-KO cells cultured in complete medium in 24-well plates were treated for 36 hours at 70% confluency with the following compounds: (**A**) 1 mM of NaI (''I'') or 1 mM of the free radical scavenger N-acetylcysteine (NAC), or both; control wells (''C'') were treated only with vehicle (water). (**B**) 20 μM of 2-iodohexadecanal or 2 or 5 μM of SLF for 24 hours. Luciferase reporter activity was determined in cell extracts from the respective conditions. Results are presented as fold activity over the respective control group treated with vehicle only. (**C–F**) PCCL3 ARE-WT or ARE-Nrf2-KO cells were treated as above and relative mRNA levels of *Tg* (**C**), *Nqo1* (**D**), *Gpx2* (**E**), and *Txnrd1* (**F**) normalized to *Rpl19* as the reference gene were quantified by real-time RT-PCR. Error bars indicate means ± standard deviation of at least three independent experiments. $^{*}p < 0.05$ vs. WT-C; $^{\#}p < 0.05$ vs. respective treated WT; n.s., not significant.

ARE cells (Fig. 6A). These data suggest that iodide exposure activates Nrf2 signaling in a ROS-dependent manner. This was further confirmed by assaying overall ROS levels using the fluorescent probe CM-H_2DCFDA in WT, Nrf2 KO, and Keap1 KO PCCL3 cells treated with iodide with or without NAC (Supplementary Fig. S10). In addition, basal ROS levels were higher in Nrf2 KO cells and lower in Keap1 KO cells (Supplementary Fig. S10).

The effects of iodide in thyroid follicular cells are believed to be exerted mainly by iodide metabolites produced via oxidative reactions with cellular lipids. One of the main active iodide intermediates is 2-IHDA (50). Thus, cells were treated with 2-IHDA (or SLF as a positive control) and ARE activity and mRNA expression levels of antioxidant genes and of Tg were assayed. Both SLF and 2-IHDA activated the ARE in WT cells (Fig. 6B). In Nrf2 KO cells, basal ARE activity was markedly reduced and inducibility by SLF, and 2-IHDA was abolished (Fig. 6B). The exact same pattern was observed in the mRNA levels of *Tg* (Fig. 6C). Similar patterns were also observed in the mRNA levels of antioxidant genes, with some specificities among them. For example, basal levels were reduced in Nrf2 KO cells for *Nqo1* and *Gpx2* (Fig. 6D and E) but not for *Txnrd1* (Fig. 6F). In all cases, inducibility by SLF and 2-IHDA was abolished in Nrf2 KO cells (Fig. 6B–F). Taken together, these data indicate that iodide and its active intermediate 2-IHDA can activate Nrf2 signaling in thyroid follicular cells and that Nrf2 activation by iodide is mediated by ROS.

Nrf2 directly controls Tg gene expression via binding to two functional AREs in a conserved upstream enhancer

Since the aforementioned data indicated transcriptional regulation of the *Tg* gene by Nrf2, the study sought to clarify the underlying mechanism. Thus, the known regulatory sequences of the human *TG* gene were analyzed, namely a proximal promoter and a distal upstream enhancer (38), for potential Nrf2 binding sites. While the proximal promoter did not contain any potential AREs, two such sequences (ARE1 and ARE2) were identified in the upstream enhancer (Fig. 7A): ARE1 lies on the forward DNA strand between −2830 and −2816 bp from the transcription start site (TSS), and ARE2 lies on the reverse strand between −3229 and −3215 bp. This human enhancer sequence is known to contain functional binding sites for thyroid transcription factor-1 (TTF1; NKX2.1), and it has been described in the human and bovine genes (39,51), but it has not been reported whether it is conserved in rodents. The sequence alignments showed that this enhancer sequence is conserved between humans, mice, and rats (Fig. 7A). Interestingly, among the known and putative regulatory elements identified, only one of the three TTF1 binding sites is conserved among these species, while a previously described putative adenosine 3′,5′-cyclic monophosphate response element–like element (52) is not conserved in rodents. In contrast, both ARE elements were also identified in the *Tg* promoter of the rat (rARE1 from −2414 to −2400, and rARE2 from −2750 to −2736) and mouse (mARE1 from −2384 to −2316, and mARE2 from −2712 to −2698). These two AREs are thus located at about the same distance from the corresponding TSS in the studied species, have a similar distance between them, and display the same orientation regarding their location on the forward (ARE1) or reverse (ARE2) DNA strand (Fig. 7A).

To test whether the predicted AREs are functional, a previously described human *TG* enhancer-promoter luciferase reporter construct was employed (38). First, it was shown that reporter activity is induced by treatment with SLF or CDDO-Im (Supplementary Fig. S11A). Next, ARE1, ARE2, or both were mutagenized in the reporter construct, introducing mutations predicted to abolish Nrf2 binding, and then transient transfection experiments were performed in PCCL3 cells. In WT cells, mutation of either ARE1 or ARE2 significantly reduced both the basal and the SLF-inducible reporter activity (Fig. 7B). Moreover, the mutation of both AREs further reduced basal reporter activity and completely abolished its inducibility by SLF (Fig. 7B). In a heterologous system (Hela cells transfected with TTF1), WT reporter activity was increased by SLF treatment, co-transfection of Nrf2, or their combination, whereas it was reduced by co-transfection of Keap1. The ARE1/2 double mutant reporter showed no response under these conditions (Supplementary Fig. S11B). Taken together, these data indicate that both AREs in the upstream Tg enhancer are transcriptionally functional. The study therefore tested for direct binding of Nrf2 to these sequences by ChIP in WT and Nrf2 KO PCCL3 cells (Fig. 7C). In WT cells, a significant enrichment of Nrf2 binding over a negative control was evident under basal conditions for both AREs, comparable to binding to a known functional ARE in the *Nqo1* gene. For both AREs, Nrf2 binding increased significantly in response to SLF treatment in WT cells. In contrast, in Nrf2 KO cells, only a background signal was detected for both AREs either under basal conditions or in response to SLF, similar to the control Nqo1 ARE (Fig. 7C). Taken together, these data demonstrate that Nrf2 can directly upregulate *Tg* gene expression via binding to two functional AREs in a conserved upstream enhancer. The main results of the above-described cell culture experiments among the different genotypes and conditions are summarized in Table 2.

Discussion

The present findings show that Nrf2 exerts pleiotropic functions in the thyroid gland (Tables 1 and 2 and Fig. 8). For some of these roles, in large part the underlying mechanisms have been elucidated here, while for others, notably regarding the effects on Tg iodination, further studies will be needed in the future. First, Nrf2 directly upregulates the transcription of the *Tg* gene via binding to two AREs in its upstream enhancer, which are conserved between rodents and human. Nrf2 thus emerges as the first ubiquitous transcription factor to regulate Tg expression. Interestingly, *Nrf2* mRNA levels in the adult human thyroid are among the highest compared to other tissues (Human Protein Atlas; https://www.proteinatlas.org/ENSG00000116044-NFE2L2/tissue#gene_information) (53). Also, during mouse development, the timing of first *Nrf2* mRNA detection in the thyroid gland (E14.5) coincides perfectly with that of *Tg* (E14.5), whereas *Ttf1* mRNA is already expressed in the gland from E12.5 (mouse Gene Expression Database, http://www.informatics.jax.org/gxd) (54). Even though patterns suggestive of increased degradation of Tg were not observed in the Nrf2 KO mice, the present data do not exclude

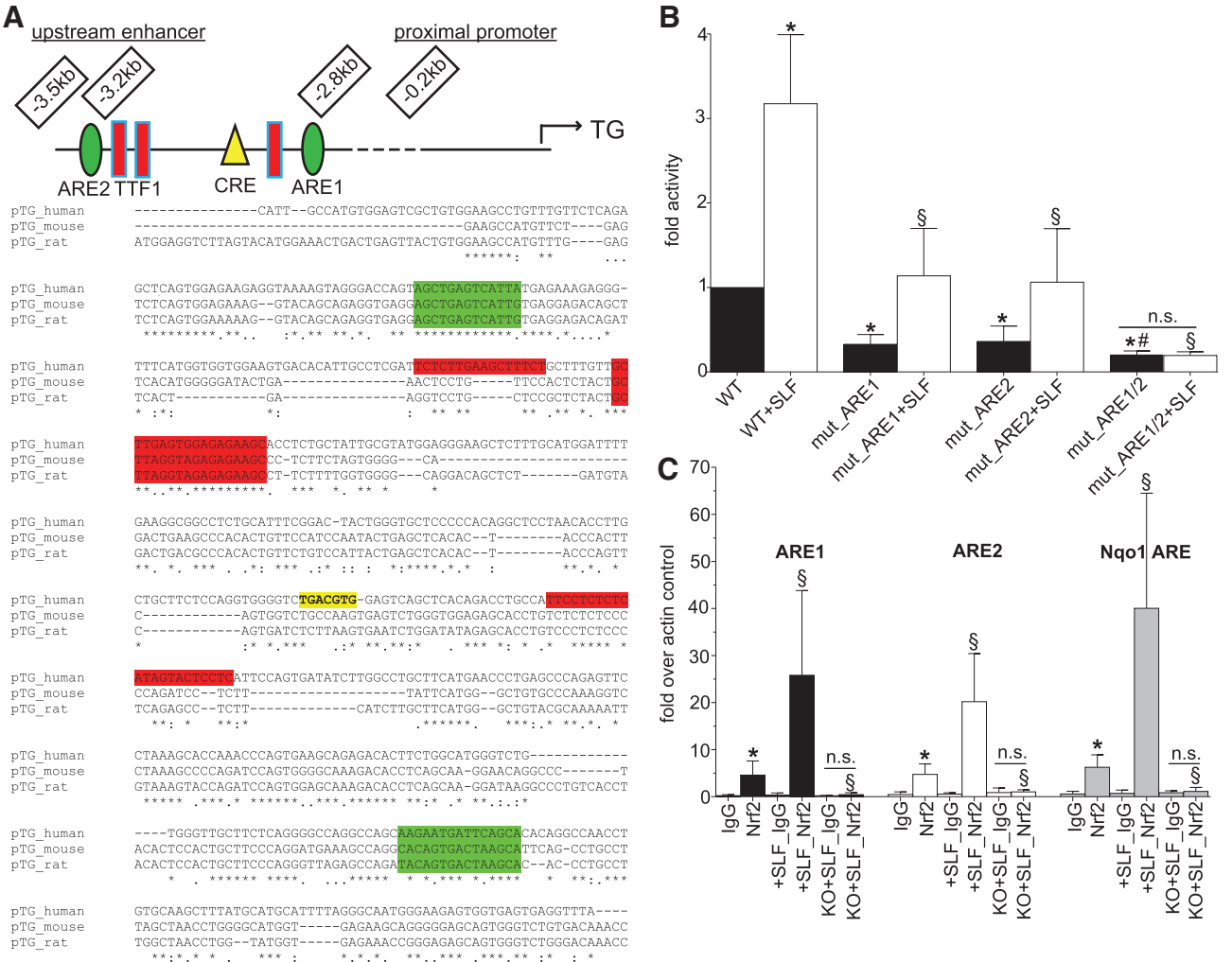

FIG. 7. Evolutionary conservation of the upstream *Tg* enhancer and regulation of its activity by direct binding of Nrf2 to two conserved AREs. (**A**) Schematic representation of the organization of the human *TG* proximal promoter and upstream enhancer. The relative positions of two newly identified AREs (ARE1 and ARE2) sites are shown (green), along with known high-affinity TTF1 binding sites (red) and a putative CRE-like site (yellow). (**B**) Functional analysis of ARE binding sites in the human Tg upstream enhancer. PCCL3 cells cultured in complete medium in 96-well plates were transfected as indicated with different constructs of human Tg promoter/enhancer (pTg) either WT or mutated in the core ARE1 or ARE2 sequences (mut_ARE1 and mut_ARE2, respectively) or in both (mut_ARE1/2). Cells were treated 24 hours later with 5 μM of SLF or vehicle (<0.1% dimethyl sulfoxide), and lysed 24 hours later to measure luciferase activity. Co-transfected pEGFP-N1 plasmid and renilla luciferase pRLTK-ΔARE plasmids allowed to evaluate the transfection efficiency and to normalize the luciferase activities, respectively. Results are presented as fold change over the normalized activity of the WT pTg construct. Error bars indicate means ± standard deviation of at least three independent experiments. $^{*}p < 0.05$ vs. WT; $^{\S}p < 0.05$ vs. WT + SLF; $^{\#}p < 0.05$ vs. mut_ARE2; n.s., not significant. (**C**) Functional validation of ARE1 and ARE2 as Nrf2 binding sites in the rat *Tg* upstream enhancer. WT or Nrf2-KO (KO) PCCL3 cells cultured in complete medium were treated with SLF or vehicle for 24 hours, as in (**B**). Chromatin was immunoprecipitated using a rabbit anti-Nrf2 antibody validated for ChIP or a control rabbit IgG. Immunoprecipitated DNA was quantified by real-time RT-PCR using primers flanking the homologous ARE1 or ARE2 site in the rat *Tg* enhancer. The validated ARE in the rat *Nqo1* promoter served as positive control, while an unrelated sequence downstream of the *Actb* gene served as negative control. Quantified DNA for each target was normalized to corresponding input DNA, and the results were plotted as fold enrichment of the target sequence over the negative control target. Error bars indicate means ± standard deviation of at least three independent experiments. $^{*}p < 0.05$ vs. respective IgG control; $^{\S}p < 0.05$ vs. respective Nrf2 untreated; n.s., not significant.

additional mechanisms that might contribute to the lower Tg levels observed in the Nrf2 KO mice, such as altered processing (55).

Regulation of Tg by a redox-responsive transcription factor makes biological sense because not only Tg iodination but also Tg folding processes are mediated by oxidation reactions. Thus, regulation of both Tg production and antioxidant defense by Nrf2 likely facilitates the coordination of these processes in order to ensure normal follicular function with optimal Tg economy. Indeed, the second function of Nrf2 under normal conditions is to prevent excessive Tg iodination. Previous studies indicate that excess iodination

TABLE 2. SUMMARY OF THE MAIN FINDINGS IN CELL LINES

	Nrf2 KO	*Keap1 KO*
Tg mRNA	↓	↑
Tg protein	↓	↑
Nqo1 (*Gpx2*, *Txrnd1*) mRNA	↓	↑
ROS	↑	↓
ARE basal activity	↓	n.t.
ARE inducible activity	↓	n.t.
Nrf2 binding to Tg AREs	↓↓	n.t.

Arrows indicate changes compared to WT cells; n.t., not tested. ROS, reactive oxygen species; ARE, antioxidant response element.

within the thyrocyte is apparently avoided by controlling the intracellular availability of H_2O_2 through glutathione peroxidase activity (56), and thioredoxin reductase has also been proposed as a means for the thyroid to detoxify H_2O_2 (57). The findings show that both these enzymes (Gpx2 and Txnrd1) are positively regulated by Nrf2, supporting a possible mechanistic link between Nrf2 and inhibition of Tg iodination metabolism. Thus, it is speculated that this might be mediated by a reduction of basal ROS levels via the control of the basal transcription of antioxidant genes (Fig. 8). However, previous work has shown that treatment of WT mice with the ROS scavenger NAC does not eliminate iodinated Tg from thyroid follicles (58). Thus, further work is necessary to elucidate the underlying mechanism. Because Tg iodination requires the 3D structure of the follicle, it cannot be modeled properly in conventional 2D cultures of thyroid follicular cells. The possibility of creating stem cell–derived 3D functional follicles (59) should make it possible to test the underlying mechanism of increased Tg iodination in Nrf2 KO thyroids in the near future.

Considering that Nrf2 has an impact on both total Tg levels and iodinated Tg levels, it is remarkable that ubiquitous and ts-Nrf2 KO mice are neither hyper- nor hypothyroid. The observed euthyroidism suggests that the levels of total Tg and iodinated Tg are in fact in a dynamic equilibrium. This would allow the thyroid to employ Nrf2-mediated antioxidant responses to preserve redox homeostasis, despite being constantly exposed to pro-oxidant substances such as H_2O_2, which is necessary for its physiological function, while at the same time maintaining normal levels of thyroid hormone production. This equilibrium is partly mediated by the regulatory actions of Nrf2 on Tg and ROS, but also apparently by a Nrf2-independent mechanism, since the equilibrium is also maintained under the extreme setting of absent Nrf2 activity (Fig. 8). Tg itself is a candidate mediator of this effect, since it has been proposed to exert multiple autoregulatory functions in thyroid follicles (60). Alternatively, altered processing of iodinated Tg in Nrf2 KO mice is another possibility that might explain the euthyroid state of the animals. Nrf2 KO mice can now serve as a sensitized background for further studies to elucidate such thyroid homeostatic mechanisms.

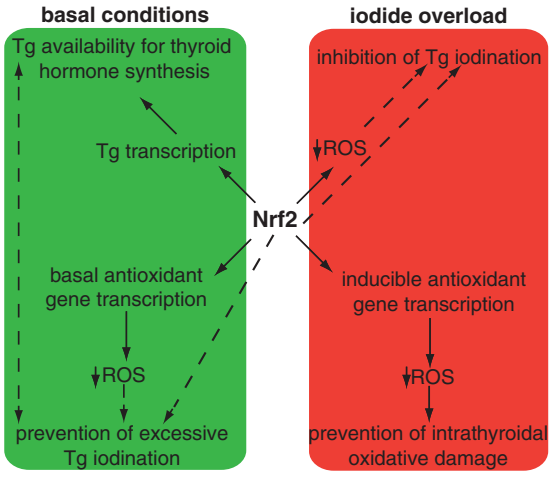

FIG. 8. Schematic representation of demonstrated and proposed pleitropic functions of Nrf2 in follicular thyroid cells under basal conditions and in response to iodide overload. The solid arrows indicate mechanisms sufficiently demonstrated in the present work. The dotted arrows indicate putative mechanisms that require further investigation.

Third, the present data indicate that the antioxidant function of Nrf2 is even more important under conditions of iodide overload, which further activate Nrf2 and its transcriptional program to limit ROS levels and thereby prevent oxidative damage to biomolecules of follicular cells, and potentially contribute to the autoregulatory reduction in H_2O_2 levels in response to high iodide (46). This latter mechanism may account for the fourth effect of Nrf2, namely its contribution to the inhibition of Tg iodination under iodide challenge. While it is known that iodide overload inhibits thyroperoxidase (TPO) activity via iodide intermediates such as 2-IHDA (61), this effect (the so-called Wolff–Chaikoff phenomenon) (47) is not yet fully elucidated. It is speculated that Nrf2, via control of ROS levels and/or other mechanisms, may impact the levels of 2-IHDA or other iodolipids that inhibit TPO activity. The availability of Nrf2 KO rats (62,63), with their bigger thyroid size that can facilitate biochemical studies, offers an opportunity to investigate the mechanism by which Nrf2 impacts iodide metabolism under basal conditions and during iodide excess.

In contrast to *Tg*, which is directly regulated by Nrf2, other genes central to thyroid follicular cell specification, differentiation, and/or function were not impacted by Nrf2 in ways indicating direct regulation. Some of them may be impacted indirectly as a result of the effect of the crosstalk of Nrf2 with other pathways or due to the general functional status of the cell. This might explain, for example, the differences observed between ubiquitous and thyroid-specific Nrf2 KO mice in the mRNA levels of *Duox1* and *Duoxa1* compared to respective controls. Similarly, *Nis* levels were either not impacted in Nrf2 loss-of-function conditions or showed a mild tendency toward lower levels, which is also suggestive of an indirect effect. Interestingly, the fact that total T4 levels were similar to controls in ts-Nrf2 KO mice but higher than controls in ubiquitous Nrf2 KO mice is suggestive of a possible role of Nrf2 in deiodinase expression and/or activity, consistent with the presence of a highly conserved putative ARE sequence of yet unknown functionality in the upstream region of the *DIO2* gene (64). However, lower mRNA levels of *Dio2* were not observed in the Nrf2 KO mice or ts-Nrf2 KO mice, but a tendency for lower *Dio1* mRNA levels was observed in Nrf2 loss-of-function conditions in mice and cells. Lastly, *Tpo* levels did not show significant differences in

mice but showed consistently lower levels in Keap1 KO cells, arguing against direct regulation by Nrf2.

Recently, it was shown that in mice lacking Nis but provided with high doses of iodide, Tg iodination and thyroid hormone synthesis can proceed successfully to a certain degree (65). In that setting, a decrease in the mRNA levels of *Nrf2* and various antioxidant genes was observed in association with high TSH levels, raising the possibility that TSH represses Nrf2 to increase ROS levels, thereby favoring the oxidative reactions required for Tg iodination and thyroid hormone synthesis (65). In the present work, patterns were observed in TSH-treated cells that are consistent with this hypothesis, including slightly reduced *Nrf2* mRNA levels, increased *Keap1* mRNA levels, and reduced ARE activity. The availability of the tool set described here, notably the Nrf2 KO and Keap1 KO cells, will allow the mechanisms by which TSH impacts Nrf2 signaling to be further characterized.

The demonstration that Nrf2 has hitherto unrecognized roles in the thyroid opens a wide field for further investigations into the relationship between antioxidant defense and thyroid pathophysiology. For example, it has been well documented that increased Tg iodination facilitates processing and presentation of a cryptic pathogenic peptide, suggesting a mechanism that can at least in part account for the association of high iodide intake with the development of autoimmune thyroid disease (66). Interestingly, when Nrf2 KO mice are bred into autoimmunity-permissive genetic backgrounds, a subset of them develop a multi-organ autoimmune syndrome (67–69), but the involvement of the thyroid has not been examined. It will thus be interesting to test whether Nrf2 KO mice in an appropriate background develop thyroid autoimmunity either spontaneously or when exposed chronically to excess iodide, as well as to investigate whether functional polymorphisms in the gene encoding Nrf2 in humans (*NFE2L2*) are associated with autoimmune Hashimoto's thyroiditis. In addition, two recent case reports have associated loss-of-function mutations in *KEAP1* with goiter (thyroid enlargement) in respective families (70,71). The finding of increased Tg levels in Keap1 KO cells suggests that this may be a mechanism contributing to the goiter phenotype. It is therefore relevant to phenotype in future work thyroid anatomy and function in Keap1 hypomorphic mice, in which Nrf2 is constitutively activated at moderate levels (72). Lastly, dietary antioxidants activating Nrf2, such as sulforaphane, are being clinically tested for the chemoprevention of diseases associated with oxidative stress (73,74). Yet, their potential beneficial, detrimental, or neutral effects on the thyroid have not been characterized. In this sense, it will be interesting to test thyroid function among participants in sulforaphane clinical trials.

To conclude, the relationship between iodide, Tg, oxidative stress, and Nrf2 is also interesting from an evolutionary perspective. Studies in kelp have shown that iodide has ancestral roles in redox homeostasis, including scavenging of atmospheric ozone (75). Nrf2 homologues with antioxidant functions are also ancient, appearing first in fungi around 1.5 billion years ago when photosynthetic oxygen was being absorbed into the oceans (76). In contrast, Tg appears to represent a novel molecular architecture elaborated as a single event at the base of vertebrates and virtually unchanged thereafter (77). Thus, it is speculated that after thyroid, Tg, and Tg iodination appeared during evolution, it was beneficial to adapt Nrf2 beyond its established antioxidant function to regulate Tg expression and iodination in harmony with the redox status of the thyroid follicular cells.

Acknowledgments

We are grateful to Prof. Roberto Di Lauro, Prof. Gabriella De Vita, Prof. Michael Sporn, and Dr. Nobunao Wakabayashi for providing valuable reagents, as well as to Prof. Dionysios Papachristou, Dr. Stavroula Manolakou, and Dr. Ioannis Lilis for expert technical assistance. This work was supported by Swiss National Science Foundation Research Grant 31003A_153062; Leenaards Foundation 2016 Fellowship for Academic Promotion in Clinical Medicine; Swiss National Science Foundation—State Secretariat for Education, Research and Innovation (SNF-COST) Project 174626—C15.0045; 3R Foundation Switzerland Project Grant 146-15; the Swiss Society for Endocrinology-Diabetology 2014 Young Independent Investigator Award; Marie Curie International Reintegration Grant 268266 (all to G.P.S.); and by grant R37DK15070 from the National Institutes of Health (to S.R.). The content is solely the responsibility of the authors and does not necessarily represent the official views of the funding agencies. The work benefited from COST Actions BM1307 (PROTEOSTASIS) and CA16112 (NutRedOx), both supported by European Cooperation in Science and Technology (COST).

Author Disclosure Statement

The authors have nothing to disclose.

References

1. Halliwell B 2007 Biochemistry of oxidative stress. Biochem Soc Trans **35:**1147–1150.
2. Jones DP 2006 Redefining oxidative stress. Antioxid Redox Signal **8:**1865–1879.
3. Maier J, van Steeg H, van Oostrom C, Karger S, Paschke R, Krohn K 2006 Deoxyribonucleic acid damage and spontaneous mutagenesis in the thyroid gland of rats and mice. Endocrinology **147:**3391–3397.
4. Leoni SG, Kimura ET, Santisteban P, De la Vieja A 2011 Regulation of thyroid oxidative state by thioredoxin reductase has a crucial role in thyroid responses to iodide excess. Mol Endocrinol **25:**1924–1935.
5. Poncin S, Gerard AC, Boucquey M, Senou M, Calderon PB, Knoops B, Lengele B, Many MC, Colin IM 2008 Oxidative stress in the thyroid gland: from harmlessness to hazard depending on the iodine content. Endocrinology **149:**424–433.
6. Poncin S, Colin IM, Gerard AC 2009 Minimal oxidative load: a prerequisite for thyroid cell function. J Endocrinol **201:**161–167.
7. Poncin S, Van Eeckoudt S, Humblet K, Colin IM, Gerard AC 2010 Oxidative stress: a required condition for thyroid cell proliferation. Am J Pathol **176:**1355–1363.
8. Maier J, van Steeg H, van Oostrom C, Paschke R, Weiss RE, Krohn K 2007 Iodine deficiency activates antioxidant genes and causes DNA damage in the thyroid gland of rats and mice. Biochim Biophys Acta **1773:**990–999.
9. Krohn K, Maier J, Paschke R 2007 Mechanisms of disease: hydrogen peroxide, DNA damage and mutagenesis in the

development of thyroid tumors. Nat Clin Pract Endocrinol Metab **3:**713–720.
10. Motohashi H, Yamamoto M 2004 Nrf2-Keap1 defines a physiologically important stress response mechanism. Trends Mol Med **10:**549–557.
11. Kang MI, Kobayashi A, Wakabayashi N, Kim SG, Yamamoto M 2004 Scaffolding of Keap1 to the actin cytoskeleton controls the function of Nrf2 as key regulator of cytoprotective phase 2 genes. Proc Natl Acad Sci U S A **101:**2046–2051.
12. Itoh K, Wakabayashi N, Katoh Y, Ishii T, Igarashi K, Engel JD, Yamamoto M 1999 Keap1 represses nuclear activation of antioxidant responsive elements by Nrf2 through binding to the amino-terminal Neh2 domain. Genes Devel **13:**76–86.
13. Dhakshinamoorthy S, Jaiswal AK 2001 Functional characterization and role of INrf2 in antioxidant response element-mediated expression and antioxidant induction of NAD(P)H:quinone oxidoreductase1 gene. Oncogene **20:** 3906–3917.
14. Katsuoka F, Motohashi H, Ishii T, Aburatani H, Engel JD, Yamamoto M 2005 Genetic evidence that small maf proteins are essential for the activation of antioxidant response element-dependent genes. Mol Cell Biol **25:**8044–8051.
15. Itoh K, Chiba T, Takahashi S, Ishii T, Igarashi K, Katoh Y, Oyake T, Hayashi N, Satoh K, Hatayama I, Yamamoto M, Nabeshima Y 1997 An Nrf2/small Maf heterodimer mediates the induction of phase II detoxifying enzyme genes through antioxidant response elements. Biochem Biophys Res Commun **236:**313–322.
16. Motohashi H, Katsuoka F, Engel JD, Yamamoto M 2004 Small Maf proteins serve as transcriptional cofactors for keratinocyte differentiation in the Keap1-Nrf2 regulatory pathway. Proc Natl Acad Sci U S A **101:**6379–6384.
17. Sykiotis GP, Bohmann D 2010 Stress-activated cap'n'collar transcription factors in aging and human disease. Sci Signal **3:**re3.
18. Lee JM, Li J, Johnson DA, Stein TD, Kraft AD, Calkins MJ, Jakel RJ, Johnson JA 2005 Nrf2, a multi-organ protector? FASEB J **19:**1061–1066.
19. Yates MS, Kwak MK, Egner PA, Groopman JD, Bodreddigari S, Sutter TR, Baumgartner KJ, Roebuck BD, Liby KT, Yore MM, Honda T, Gribble GW, Sporn MB, Kensler TW 2006 Potent protection against aflatoxin-induced tumorigenesis through induction of Nrf2-regulated pathways by the triterpenoid 1-[2-cyano-3-,12-dioxooleana-1,9(11)-dien-28-oyl]imidazole. Cancer Res **66:**2488–2494.
20. Xu C, Huang MT, Shen G, Yuan X, Lin W, Khor TO, Conney AH, Kong AN 2006 Inhibition of 7,12-dimethylbenz(a)anthracene-induced skin tumorigenesis in C57BL/6 mice by sulforaphane is mediated by nuclear factor E2-related factor 2. Cancer Res **66:**8293–8296.
21. Ramos-Gomez M, Kwak MK, Dolan PM, Itoh K, Yamamoto M, Talalay P, Kensler TW 2001 Sensitivity to carcinogenesis is increased and chemoprotective efficacy of enzyme inducers is lost in nrf2 transcription factor-deficient mice. Proc Natl Acad Sci U S A **98:**3410–3415.
22. Wang T, Liang X, Abeysekera IR, Iqbal U, Duan Q, Naha G, Lin L, Yao X 2017 Activation of the Nrf2-keap 1 pathway in short-term iodide excess in thyroid in rats. Oxid Med Cell Longev **2017:**4383652.
23. Bouchard M, Souabni A, Busslinger M 2004 Tissue-specific expression of cre recombinase from the Pax8 locus. Genesis **38:**105–109.
24. Reddy NM, Potteti HR, Mariani TJ, Biswal S, Reddy SP 2011 Conditional deletion of Nrf2 in airway epithelium exacerbates acute lung injury and impairs the resolution of inflammation. Am J Respir Cell Mol Biol **45:**1161–1168.
25. Ferrara AM, Liao XH, Gil-Ibanez P, Marcinkowski T, Bernal J, Weiss RE, Dumitrescu AM, Refetoff S 2013 Changes in thyroid status during perinatal development of MCT8-deficient male mice. Endocrinology **154:**2533–2541.
26. Ziros PG, Chartoumpekis DV, Sykiotis GP 2016 A simple protocol for high efficiency protein isolation after RNA isolation from mouse thyroid and other very small tissue samples. Methods Mol Biol **1449:**383–393.
27. Ziros PG, Manolakou SD, Habeos IG, Lilis I, Chartoumpekis DV, Koika V, Soares P, Kyriazopoulou VE, Scopa CD, Papachristou DJ, Sykiotis GP 2013 Nrf2 is commonly activated in papillary thyroid carcinoma, and it controls antioxidant transcriptional responses and viability of cancer cells. J Clin Endocrinol Metab **98:**E1422–1427.
28. Den Hartog MT, De Boer M, Veenboer GJ, De Vijlder JJ 1990 Generation and characterization of monoclonal antibodies directed against noniodinated and iodinated thyroglobulin, among which are antibodies against hormonogenic sites. Endocrinology **127:**3160–3165.
29. Levy O, Dai G, Riedel C, Ginter CS, Paul EM, Lebowitz AN, Carrasco N 1997 Characterization of the thyroid Na+/I– symporter with an anti-COOH terminus antibody. Proc Natl Acad Sci U S A **94:**5568–5573.
30. Fusco A, Berlingieri MT, Di Fiore PP, Portella G, Grieco M, Vecchio G 1987 One- and two-step transformations of rat thyroid epithelial cells by retroviral oncogenes. Mol Cell Biol **7:**3365–3370.
31. Liby K, Hock T, Yore MM, Suh N, Place AE, Risingsong R, Williams CR, Royce DB, Honda T, Honda Y, Gribble GW, Hill-Kapturczak N, Agarwal A, Sporn MB 2005 The synthetic triterpenoids, CDDO and CDDO-imidazolide, are potent inducers of heme oxygenase-1 and Nrf2/ARE signaling. Cancer Res **65:**4789–4798.
32. Ren D, Villeneuve NF, Jiang T, Wu T, Lau A, Toppin HA, Zhang DD 2011 Brusatol enhances the efficacy of chemotherapy by inhibiting the Nrf2-mediated defense mechanism. Proc Natl Acad Sci U S A **108:**1433–1438.
33. Pereira A, Braekman JC, Dumont JE, Boeynaems JM 1990 Identification of a major iodolipid from the horse thyroid gland as 2-iodohexadecanal. J Biol Chem **265:**17018–17025.
34. Favreau LV, Pickett CB 1995 The rat quinone reductase antioxidant response element. Identification of the nucleotide sequence required for basal and inducible activity and detection of antioxidant response element-binding proteins in hepatoma and non-hepatoma cell lines. J Biol Chem **270:** 24468–24474.
35. Wakabayashi N, Dinkova-Kostova AT, Holtzclaw WD, Kang MI, Kobayashi A, Yamamoto M, Kensler TW, Talalay P 2004 Protection against electrophile and oxidant stress by induction of the phase 2 response: fate of cysteines of the Keap1 sensor modified by inducers. Proc Natl Acad Sci U S A **101:**2040–2045.
36. Dreos R, Ambrosini G, Groux R, Cavin Perier R, Bucher P 2017 The eukaryotic promoter database in its 30th year: focus on non-vertebrate organisms. Nucleic Acids Res **45:** D51–D55.
37. Mathelier A, Fornes O, Arenillas DJ, Chen CY, Denay G, Lee J, Shi W, Shyr C, Tan G, Worsley-Hunt R, Zhang AW, Parcy F, Lenhard B, Sandelin A, Wasserman WW 2016

JASPAR 2016: a major expansion and update of the open-access database of transcription factor binding profiles. Nucleic Acids Res **44:**D110–115.
38. Pohlenz J, Dumitrescu A, Zundel D, Martine U, Schonberger W, Koo E, Weiss RE, Cohen RN, Kimura S, Refetoff S 2002 Partial deficiency of thyroid transcription factor 1 produces predominantly neurological defects in humans and mice. J Clin Invest **109:**469–473.
39. Berg V, Vassart G, Christophe D 1996 Identification of a thyroid-specific and cAMP-responsive enhancer in the upstream sequences of the human thyroglobulin promoter. Biochim Biophys Acta **1307:**35–38.
40. Donda A, Javaux F, Van Renterghem P, Gervy-Decoster C, Vassart G, Christophe D 1993 Human, bovine, canine and rat thyroglobulin promoter sequences display species-specific differences in an *in vitro* study. Mol Cell Endocrinol **90:**R23–26.
41. Cong L, Ran FA, Cox D, Lin S, Barretto R, Habib N, Hsu PD, Wu X, Jiang W, Marraffini LA, Zhang F 2013 Multiplex genome engineering using CRISPR/Cas systems. Science **339:**819–823.
42. Wakabayashi N, Shin S, Slocum SL, Agoston ES, Wakabayashi J, Kwak MK, Misra V, Biswal S, Yamamoto M, Kensler TW 2010 Regulation of notch1 signaling by Nrf2: implications for tissue regeneration. Sci Signal **3:**ra52.
43. Runkle EA, Rice SJ, Qi J, Masser D, Antonetti DA, Winslow MM, Mu D 2012 Occludin is a direct target of thyroid transcription factor-1 (TTF-1/NKX2-1). J Biol Chem **287:** 28790–28801.
44. Cleries R, Galvez J, Espino M, Ribes J, Nunes V, de Heredia ML 2012 BootstRatio: a web-based statistical analysis of fold-change in qPCR and RT-qPCR data using resampling methods. Comput Biol Med **42:**438–445.
45. Eng PH, Cardona GR, Fang SL, Previti M, Alex S, Carrasco N, Chin WW, Braverman LE 1999 Escape from the acute Wolff–Chaikoff effect is associated with a decrease in thyroid sodium/iodide symporter messenger ribonucleic acid and protein. Endocrinology **140:**3404–3410.
46. Kopp P 2005 Thyroid hormone synthesis. In: Braverman LE, Utiger RD (eds) Werner and Ingbar's The Thyroid: A Fundamental and Clinical Text. Lippincott Williams & Wilkins, Philadelphia, PA, pp 48–74.
47. Wolff J, Chaikoff IL 1948 Plasma inorganic iodide as a homeostatic regulator of thyroid function. J Biol Chem **174:** 555–564.
48. Santisteban P, Kohn LD, Di Lauro R 1987 Thyroglobulin gene expression is regulated by insulin and insulin-like growth factor I, as well as thyrotropin, in FRTL-5 thyroid cells. J Biol Chem **262:**4048–4052.
49. Santisteban P, Acebron A, Polycarpou-Schwarz M, Di Lauro R 1992 Insulin and insulin-like growth factor I regulate a thyroid-specific nuclear protein that binds to the thyroglobulin promoter. Mol Endocrinol **6:**1310–1317.
50. Panneels V, Juvenal G, Boeynaems JM, Dumont JE, Van Sande J 2009 Iodide effects on the thyroid: biochemical, physiological, pharmacological, and clinical effects of iodide in the thyroid. In: Preedy VR, Burrow GN, Watson R (eds) Comprehensive Handbook of Iodine. Academic Press, Oxford, pp 303–314.
51. Christophe-Hobertus C, Christophe D 1999 Two binding sites for thyroid transcription factor 1 (TTF-1) determine the activity of the bovine thyroglobulin gene upstream enhancer element. Mol Cell Endocrinol **149:**79–84.
52. Berg V, Vassart G, Christophe D 1997 A zinc-dependent DNA-binding activity co-operates with cAMP-responsive-element-binding protein to activate the human thyroglobulin enhancer. Biochem J **323:**349–357.
53. Uhlen M, Fagerberg L, Hallstrom BM, Lindskog C, Oksvold P, Mardinoglu A, Sivertsson A, Kampf C, Sjostedt E, Asplund A, Olsson I, Edlund K, Lundberg E, Navani S, Szigyarto CA, Odeberg J, Djureinovic D, Takanen JO, Hober S, Alm T, Edqvist PH, Berling H, Tegel H, Mulder J, Rockberg J, Nilsson P, Schwenk JM, Hamsten M, von Feilitzen K, Forsberg M, Persson L, Johansson F, Zwahlen M, von Heijne G, Nielsen J, Ponten F 2015 Proteomics. Tissue-based map of the human proteome. Science **347:** 1260419.
54. Finger JH, Smith CM, Hayamizu TF, McCright IJ, Xu J, Law M, Shaw DR, Baldarelli RM, Beal JS, Blodgett O, Campbell JW, Corbani LE, Lewis JR, Forthofer KL, Frost PJ, Giannatto SC, Hutchins LN, Miers DB, Motenko H, Stone KR, Eppig JT, Kadin JA, Richardson JE, Ringwald M 2017 The mouse Gene Expression Database (GXD): 2017 update. Nucleic Acids Res **45:**D730–D736.
55. Di Jeso B, Arvan P 2016 Thyroglobulin from molecular and cellular biology to clinical endocrinology. Endocr Rev **37:**2–36.
56. Ekholm R, Bjorkman U 1997 Glutathione peroxidase degrades intracellular hydrogen peroxide and thereby inhibits intracellular protein iodination in thyroid epithelium. Endocrinology **138:**2871–2878.
57. Howie AF, Arthur JR, Nicol F, Walker SW, Beech SG, Beckett GJ 1998 Identification of a 57-kilodalton selenoprotein in human thyrocytes as thioredoxin reductase and evidence that its expression is regulated through the calcium-phosphoinositol signaling pathway. J Clin Endocrinol Metab **83:**2052–2058.
58. Poncin S, Colin IM, Decallonne B, Clinckspooor I, Many MC, Denef JF, Gerard AC 2010 N-acetylcysteine and 15 deoxy-{delta}12,14-prostaglandin J2 exert a protective effect against autoimmune thyroid destruction *in vivo* but not against interleukin-1{alpha}/interferon {gamma}-induced inhibitory effects in thyrocytes *in vitro*. Am J Pathol **177:** 219–228.
59. Antonica F, Kasprzyk DF, Opitz R, Iacovino M, Liao XH, Dumitrescu AM, Refetoff S, Peremans K, Manto M, Kyba M, Costagliola S 2012 Generation of functional thyroid from embryonic stem cells. Nature **491:**66–71.
60. Sellitti DF, Suzuki K 2014 Intrinsic regulation of thyroid function by thyroglobulin. Thyroid **24:**625–638.
61. Rossich LE, Thomasz L, Nicola JP, Nazar M, Salvarredi LA, Pisarev M, Masini-Repiso AM, Christophe-Hobertus C, Christophe D, Juvenal GJ 2016 Effects of 2-iodohexadecanal in the physiology of thyroid cells. Mol Cell Endocrinol **437:** 292–301.
62. Taguchi K, Takaku M, Egner PA, Morita M, Kaneko T, Mashimo T, Kensler TW, Yamamoto M 2016 Generation of a new model rat: Nrf2 knockout rats are sensitive to aflatoxin B1 toxicity. Toxicol Sci **152:**40–52.
63. Priestley JR, Kautenburg KE, Casati MC, Endres BT, Geurts AM, Lombard JH 2016 The NRF2 knockout rat: a new animal model to study endothelial dysfunction, oxidant stress, and microvascular rarefaction. Am J Physiol Heart Circ Physiol **310:**H478–487.
64. Wang X, Tomso DJ, Chorley BN, Cho HY, Cheung VG, Kleeberger SR, Bell DA 2007 Identification of polymor-

phic antioxidant response elements in the human genome. Hum Mol Genet **16:**1188–1200.
65. Ferrandino G, Kaspari RR, Reyna-Neyra A, Boutagy NE, Sinusas AJ, Carrasco N 2017 An extremely high dietary iodide supply forestalls severe hypothyroidism in Na+/I– symporter (NIS) knockout mice. Sci Rep **7:**5329.
66. Dai YD, Rao VP, Carayanniotis G 2002 Enhanced iodination of thyroglobulin facilitates processing and presentation of a cryptic pathogenic peptide. J Immunol **168:**5907–5911.
67. Yoh K, Itoh K, Enomoto A, Hirayama A, Yamaguchi N, Kobayashi M, Morito N, Koyama A, Yamamoto M, Takahashi S 2001 Nrf2-deficient female mice develop lupus-like autoimmune nephritis. Kidney Int **60:**1343–1353.
68. Li J, Stein TD, Johnson JA 2004 Genetic dissection of systemic autoimmune disease in Nrf2-deficient mice. Physiol Genomics **18:**261–272.
69. Ma Q, Battelli L, Hubbs AF 2006 Multiorgan autoimmune inflammation, enhanced lymphoproliferation, and impaired homeostasis of reactive oxygen species in mice lacking the antioxidant-activated transcription factor Nrf2. Am J Pathol **168:**1960–1974.
70. Teshiba R, Tajiri T, Sumitomo K, Masumoto K, Taguchi T, Yamamoto K 2013 Identification of a KEAP1 germline mutation in a family with multinodular goitre. PloS One **8:** e65141.
71. Nishihara E, Hishinuma A, Kogai T, Takada N, Hirokawa M, Fukata S, Ito M, Yabuta T, Nishikawa M, Nakamura H, Amino N, Miyauchi A 2016 A novel germline mutation of KEAP1 (R483H) associated with a non-toxic multinodular goiter. Front Endocrinol (Lausanne) **7:**131.
72. Taguchi K, Maher JM, Suzuki T, Kawatani Y, Motohashi H, Yamamoto M 2010 Genetic analysis of cytoprotective functions supported by graded expression of Keap1. Mol Cell Biol **30:**3016–3026.
73. Egner PA, Chen JG, Wang JB, Wu Y, Sun Y, Lu JH, Zhu J, Zhang YH, Chen YS, Friesen MD, Jacobson LP, Munoz A, Ng D, Qian GS, Zhu YR, Chen TY, Botting NP, Zhang Q, Fahey JW, Talalay P, Groopman JD, Kensler TW 2011 Bioavailability of sulforaphane from two broccoli sprout beverages: results of a short-term, cross-over clinical trial in Qidong, China. Cancer Prev Res **4:**384–395.
74. Yang L, Palliyaguru DL, Kensler TW 2016 Frugal chemoprevention: targeting Nrf2 with foods rich in sulforaphane. Semin Oncol **43:**146–153.
75. Kupper FC, Carpenter LJ, McFiggans GB, Palmer CJ, Waite TJ, Boneberg EM, Woitsch S, Weiller M, Abela R, Grolimund D, Potin P, Butler A, Luther GW 3rd, Kroneck PM, Meyer-Klaucke W, Feiters MC 2008 Iodide accumulation provides kelp with an inorganic antioxidant impacting atmospheric chemistry. Proc Natl Acad Sci U S A **105:** 6954–6958.
76. Gacesa R, Dunlap WC, Barlow DJ, Laskowski RA, Long PF 2016 Rising levels of atmospheric oxygen and evolution of Nrf2. Sci Rep **6:**27740.
77. Holzer G, Morishita Y, Fini JB, Lorin T, Gillet B, Hughes S, Tohme M, Deleage G, Demeneix B, Arvan P, Laudet V 2016 Thyroglobulin represents a novel molecular architecture of vertebrates. J Biol Chem **291:**16553–16566.

Address correspondence to:
Gerasimos P. Sykiotis, MD, PhD
Service of Endocrinology, Diabetology and Metabolism
Lausanne University Hospital
Ave de la Sallaz 8, 1011 Lausanne
Switzerland

E-mail: gerasimos.sykiotis@chuv.ch